

University of Missouri, St. Louis

IRL @ UMSL

---

Chemistry & Biochemistry Faculty Works

Chemistry and Biochemistry

---


February 2019

## Biosensor Applications of Electrodeposited Nanostructures

Keith Stine

University of Missouri-St. Louis, [kstine@umsl.edu](mailto:kstine@umsl.edu)

Follow this and additional works at: <https://irl.umsl.edu/chemistry-faculty>

 Part of the [Chemistry Commons](#)

---

### Recommended Citation

Stine, Keith, "Biosensor Applications of Electrodeposited Nanostructures" (2019). *Chemistry & Biochemistry Faculty Works*. 58.

DOI: <https://doi.org/10.3390/app9040797>

Available at: <https://irl.umsl.edu/chemistry-faculty/58>

This Article is brought to you for free and open access by the Chemistry and Biochemistry at IRL @ UMSL. It has been accepted for inclusion in Chemistry & Biochemistry Faculty Works by an authorized administrator of IRL @ UMSL. For more information, please contact [marvinh@umsl.edu](mailto:marvinh@umsl.edu).

Review

# Biosensor Applications of Electrodeposited Nanostructures

Keith J. Stine

Department of Chemistry and Biochemistry, University of Missouri–Saint Louis, Saint Louis, MO 63121, USA; kstine@umsl.edu Tel.: +1-314-516-5346

Received: 22 December 2018; Accepted: 15 February 2019; Published: 24 February 2019



**Abstract:** The development of biosensors for a range of analytes from small molecules to proteins to oligonucleotides is an intensely active field. Detection methods based on electrochemistry or on localized surface plasmon responses have advanced through using nanostructured electrodes prepared by electrodeposition, which is capable of preparing a wide range of different structures. Supported nanoparticles can be prepared by electrodeposition through applying fixed potentials, cycling potentials, and fixed current methods. Nanoparticle sizes, shapes, and surface densities can be controlled, and regular structures can be prepared by electrodeposition through templates. The incorporation of multiple nanomaterials into composite films can take advantage of the superior and potentially synergistic properties of each component. Nanostructured electrodes can provide supports for enzymes, antibodies, or oligonucleotides for creating sensors against many targets in areas such as genomic analysis, the detection of protein antigens, or the detection of small molecule metabolites. Detection can also be performed using electrochemical methods, and the nanostructured electrodes can greatly enhance electrochemical responses by carefully designed schemes. Biosensors based on electrodeposited nanostructures can contribute to the advancement of many goals in bioanalytical and clinical chemistry.

**Keywords:** nanomaterials; nanostructure; nanoparticle; electrodeposition; biosensor

## 1. Introduction

Electrodeposition can be used to form nanostructures on electrode surfaces, offering a wide variety of morphologies such as supported isolated nanoparticles, regular structures formed on templates, isolated nanostructures with high degrees of ramification or variable shapes, and complex multicomponent composite structures. Each type of structure can present benefits for application as a supporting material for biosensor development resulting from properties that increase surface area, enhance electron transfer, support localized surface plasmons, or allow for improvements in the oriented immobilization of complex biomolecules. An especially interesting feature of nanostructured electrodes is their use as third-generation electrochemical biosensors, where a direct electron transfer between the electrode surface and the redox centers of the immobilized biomolecules takes place, as has recently been reviewed [1]. The formation of nanostructures by electrodeposition for use as supports for biosensor development is the focus of this review. The formation of nanostructures by alloy electrodeposition followed by dealloying to produce nanoporous gold and related materials for biomolecule immobilization is another large field; however, this has been the subject of other reviews [2,3], and thus is not a focus here. This review also does not focus on other applications of electrodeposited nanostructures outside of biosensing, or on structures formed by electroless deposition. The types of electrodes that are considered here fall into broad categories of spherical or quasi-spherical nanoparticles that are directly electrodeposited onto a supporting electrode, nanoparticles electrodeposited through or onto some form of template, electrodeposition carried

out under conditions that produced ramified or dendritic morphologies, and the electrodeposition of composite electrodes containing nanoparticles along with other components such as graphene or polymers. Some of the systems described here may fall into more than one category, and have been noted regarding their most dominant feature.

## 2. Biosensor Application of Electrodeposited Nanoparticles

The modification of electrodes with metallic nanoparticles, which are most frequently gold, provides an increase in surface area, and for enzymes, it often promotes direct electron transfer between the metal surface and the enzyme active site [1]. Approaches that do not involve electrodeposition involve the immobilization of preformed gold nanoparticles onto the electrode surface, which is often modified with the terminal amine group presenting self-assembled monolayers (SAMs) by adsorption from solution [4,5]. The immobilization of preformed nanoparticles can also apply to the nanoparticles of other metals, such as silver [6,7]. The direct formation of the gold nanoparticles on the supporting electrode by the reduction of most commonly  $\text{HAuCl}_4$  dissolved in solution is an attractive and convenient way to directly produce immobilized gold nanoparticles on an electrode surface [8]. The direct formation of nanoparticles of other metals requires the use of the appropriate precursor [9], and for alloy nanoparticles, a mixed solution of precursors for each metal [10]. Adjustment of variables and conditions can result in different outcomes for electrodeposition in terms of particle size, the surface density of particles, and morphology. The supporting electrode material, composition of the solution, temperature, and addition of structure-directing agents may all be varied. The electrochemical method that is used (fixed potential, swept or cycled potential, constant current) can be varied along with the time, potential limits, and scan rates.

### 2.1. Deposition at a Constant Potential for a Fixed Time Period

The formation of metal nanoparticles by electrodeposition at a constant applied potential for a fixed period of time is a popular strategy. The electrodeposition potential for  $\text{HAuCl}_4$  to Au in aqueous solution is 0.853 V (versus standard hydrogen electrode, SHE) [11]. Glassy carbon, which has the advantage of a wide potential window [12], is a popular choice for the supporting electrode. For example, a biosensor for the anti-cancer agent vinblastine was constructed by first electrodepositing gold nanoparticles onto a glassy carbon electrode (GCE) [13]. Electrodeposition was carried out in 3 mM of  $\text{HAuCl}_4$  and 0.5 M of  $\text{H}_2\text{SO}_4$  at  $-0.20$  V (versus Ag/AgCl) for 220 s. Scanning electron microscopy (SEM, MIRA3, TESCAN, Brno–Kohoutovice, Czech Republic) revealed a layer of gold nanoparticles of fairly uniform coverage; some of the nanoparticles were irregular in shape or in contact with their neighbors, and each of them was about 20 nm in size, as shown in Figure 1.

The gold nanoparticles were then surface modified by 3-mercaptopropionic acid, which was then covalently conjugated to tubulin using 1-ethyl-3-(3-dimethylaminopropyl) carbodiimide and N-hydroxysuccinimide (EDC/NHS) coupling reagents. Using Faradaic electrochemical impedance spectroscopy in phosphate buffer of pH 7.4 containing the redox probe 2.0 mM  $[\text{Fe}(\text{CN})_6]^{3-/4-}$ , the shift in charge transfer resistance versus vinblastine concentration was found to show two linear regions, one from 0.4 to 12.0 nM, and another from 12.0 to 65.0 nM. The detection limit for vinblastine was found to be 0.084 nM.

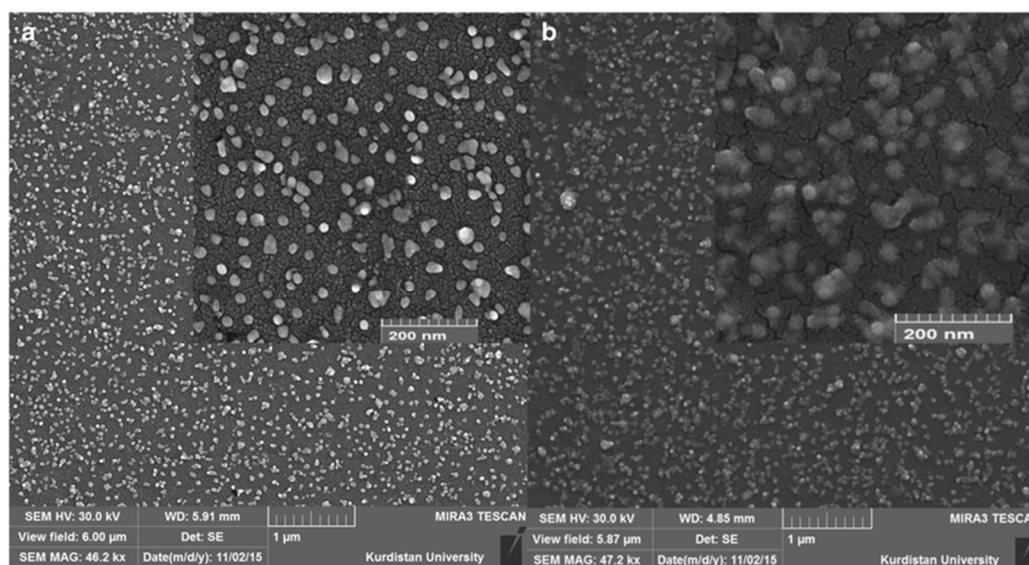


**Figure 1.** (a) SEM images of gold nanoparticles formed on glassy carbon electrode (GCE) by electrodeposition at  $-0.2$  V and 220 s from three mM of  $\text{HAuCl}_4$  and 0.5 M of  $\text{H}_2\text{SO}_4$ . (b) SEM image after surface modification with 3-mercaptopropionic acid and conjugation to tubulin. Reproduced with permission from ref. [13], Copyright 2009, Springer.

Enzymatic biosensors based on gold nanoparticles directly electrodeposited on GCE or related substrates have been prepared. Gold nanoparticles were electrodeposited onto GCE and used as a support for the enzyme horseradish peroxidase (HRP), both in native form and in a form that had been chemically conjugated to lactose [14]. The gold nanoparticles were electrodeposited at  $-0.2$  V (versus Ag/AgCl) for 60 s onto a GCE from  $100 \text{ mg L}^{-1}$  of  $\text{HAuCl}_4$  solution. SEM (JSM-7500F, JEOL USA Inc., Peabody, MA, USA) showed the gold nanoparticles with an average diameter of 100 nm covering much of the electrode surface. The lactosylated form of the enzyme was found to show greater electrocatalytic activity for hydroquinone in the presence of  $200 \text{ } \mu\text{M}$  of  $\text{H}_2\text{O}_2$ , having a detection limit of  $74 \text{ nM}$  versus  $83 \text{ nM}$  for the native enzyme. Hydroquinone is more commonly used as a redox mediator. A significant feature was that the immobilized lactosylated enzyme was more stable, retaining 60% of its activity over four months of storage versus only 10% retained activity for the native enzyme. In another example, gold nanoparticles electrodeposited onto graphite electrodes were used as a support for acetylcholinesterase and to make an amperometric assay for thiocholine [15]. The Au nanoparticles were electrodeposited from  $50 \text{ mM}$  of tetrachloroauric(III) acid ( $\text{HAuCl}_4$ ) in  $0.1 \text{ M}$  of HCl at  $-0.155 \text{ V}$  (versus Ag/AgCl) for 10 s. Acetylcholinesterase converted acetylthiocholine to acetic acid and thiocholine, and thiocholine was oxidized at  $0.8 \text{ V}$ . The detection limit for thiocholine was  $2.5 \text{ } \mu\text{M}$ , and the response was linear up to  $600 \text{ } \mu\text{M}$ . The activity of the immobilized enzyme was inhibited by the insecticide monocrotophos. Using a one-step electrodeposition, both gold nanoparticles and HRP were deposited on a GCE [16]. Electrodeposition was conducted from a solution that was  $1 \text{ mM}$  of  $\text{HAuCl}_4$ ,  $10 \text{ mM}$  of cetyltrimethylammonium bromide (CTAB), and  $3 \text{ mg L}^{-1}$  of HRP in pH 7.5 phosphate buffer at  $-0.5 \text{ V}$  (versus Ag/AgCl) for 50 mins. In the absence of CTAB and HRP, the deposited nanoparticles appeared aggregated under SEM (JSM-6701F, JEOL Ltd., Tokyo, Japan) while the addition of CTAB produced a deposit of uniformly dispersed nanoparticles that were about  $10 \text{ nm}$  in diameter. Electrodeposition including CTAB and HRP gave a deposited layer of aggregated nanoparticles, which was attributed to the electrostatic interaction between CTAB and HRP. The amperometric response to  $\text{H}_2\text{O}_2$  was greatest at pH 7.0 for the 50-minute deposition time and an operating potential of  $-0.3 \text{ V}$ . Cyclic voltammetry (CV) data indicated that multilayers of HRP were formed, as the peak current was 23 times the value that was expected for monolayer coverage. Direct electron transfer between HRP and gold was found, and the electrode could detect  $\text{H}_2\text{O}_2$  (detection limit =  $0.23 \text{ } \mu\text{M}$ , linear range  $0.5$  to  $105 \text{ } \mu\text{M}$ ), *t*-butyl hydroperoxide (detection limit =  $8.6 \text{ } \mu\text{M}$ , linear

range 10 to 1000  $\mu\text{M}$ ), and cumene hydroperoxide (detection limit = 3.6  $\mu\text{M}$ , linear range 10 to 750  $\mu\text{M}$ ). A biosensor for the antibiotic tetracycline was constructed by immobilized thiolated aptamer onto gold nanoparticles directly electrodeposited onto GCE [17]. The gold nanoparticles were electrodeposited at  $-0.2$  V (versus saturated calomel electrode, SCE) from 3 mM of  $\text{HAuCl}_4$  for 200 s. The result was coverage of the surface with irregularly shaped nanoparticles. Methylene blue redox indicator bound to the aptamer was displaced by tetracycline, resulting in a decrease in the redox current. A detection limit of  $0.42 \times 10^{-11}$  M was found, as was good recovery and the detection of tetracycline spiked into milk at concentrations of  $5 \times 10^{-9}$  M,  $5 \times 10^{-7}$  M, and  $5 \times 10^{-5}$  M.

Gold nanoparticles electrodeposited onto gold electrodes have also been used as supports for biosensor development. An electrochemical sensor for protein casein kinase II (CK2) activity was constructed using gold nanoparticles electrodeposited onto a gold electrode [18]. The electrodeposition was carried out at  $-0.2$  V (versus Ag/AgCl) for 250 s in a solution of three mM of  $\text{HAuCl}_4$  containing 0.1 M of  $\text{KNO}_3$ . A substrate peptide (CDDDDDSDDDA) for carboxypeptidase Y (CPY) was immobilized onto the gold nanoparticles. Phosphorylation of the substrate peptide hindered the CPY activity, and the response of the  $[\text{Fe}(\text{CN})_6]^{3-/4-}$  redox probe did not increase as much when a phosphorylated substrate peptide was exposed to CPY as when a non-phosphorylated substrate peptide was exposed to CPY. The scheme was used to determine an  $\text{IC}_{50}$  value of 39.77 nM for ellagic acid, which is an inhibitor of CK2.

An electrodeposited film resembling nanoporous gold, but not requiring a dealloying process, was formed by the electrodeposition of gold nanoparticles onto a Si surface onto which five nm of Ti and 43 nm of Au had been deposited by magnetron sputter coating [19]. Electrodeposition from 10 mM of  $\text{HAuCl}_4$  solution containing polyethylene glycol (PEG, 200 MW) at  $-1.3$  V (versus Ag/AgCl) for 30 s resulted in a 150-nm thick film of interconnected Au nanoparticles presenting pores of 30-nm diameter. The electrode had a detection limit of 100 nM for the oxidation of dopamine in the presence of 10  $\mu\text{M}$  of ascorbic acid and 1 mM of uric acid, as determined using the peak currents from differential pulse voltammetry (DPV) scans.

The electrodeposition of gold onto gold-coated glass slides by the application of two sequential fixed potentials was found to result in a surface morphology resembling a pile of brick-like shapes [20]. The deposition condition of  $-1.2$  V (versus Ag/AgCl) for 60 s, followed by  $-1.6$  V for 30 s from 50 mM of  $\text{KAu}(\text{CN})_2$  in 0.25 M of  $\text{Na}_2\text{CO}_3$  was found to give localized surface plasmon absorbance, which was measured in reflectivity experiments, and had a response of  $100 \pm 2$  nm of  $\text{RIU}^{-1}$  ( $\text{RIU}$  = refractive index units) and a figure of merit of 1.7. The binding of lectin concanavalin A to mixed SAMs of a thiolated mannoside (8-mercaptooctyl  $\alpha$ -D-mannopyranoside) and 3-mercapto-(triethyleneglycol) caused a red shift of the plasmon absorbance, and the binding could be followed in real-time.

## 2.2. Electrodeposition during Potential Sweeps or Cycles

In many recent applications, gold nanoparticles were electrodeposited during potential sweeps or multiple CV cycles. It has been proposed that the use of potential sweeps and cycles provides better control over particle nucleation and growth, and results in a more regularly spaced deposition of particles that are closer to uniformly shaped [21]. The potential limits, scan rate, and number of cycles can all be adjusted in this approach in addition to the variables of choice of substrate and solution composition. Figure 2 shows the SEM (S-4700, Hitachi, Tokyo, Japan) micrographs of gold nanoparticles of different sizes deposited onto indium tin oxide (ITO) glass using potential cycling. The plasmon absorbance spectra for these deposited nanoparticles are also shown. Three different preparations of nanoparticles were supported. Electrodeposition by 20 cycles at  $50$   $\text{mV sec}^{-1}$  between  $0.3$  V and  $-0.5$  V (versus SCE) resulted in particles with an average size of 90 nm from a solution of one mM of  $\text{HAuCl}_4$  at pH 2. The addition of 0.05 M of KCl to the solution increased the average particle size under these conditions to 90 nm. Larger particles with an average size of 137 nm were electrodeposited by applying 80 cycles at  $0.05$   $\text{mV sec}^{-1}$  from  $0.3$  V to  $-0.85$  V from one mM of  $\text{HAuCl}_4$  at pH 2. The refractive index sensitivity for the nanoparticles were  $45$   $\text{nm RIU}^{-1}$ ,  $137$   $\text{nm RIU}^{-1}$ , and

187 nm RIU<sup>-1</sup> for the 35-nm, 90-nm, and 137-nm particles, respectively. In comparison to the deposited particles shown in Figure 1, which were electrodeposited at a constant potential, it can be seen that the particles in Figure 2 have more regular spacing, fewer indications of neighboring particles near contact, and more uniform size.

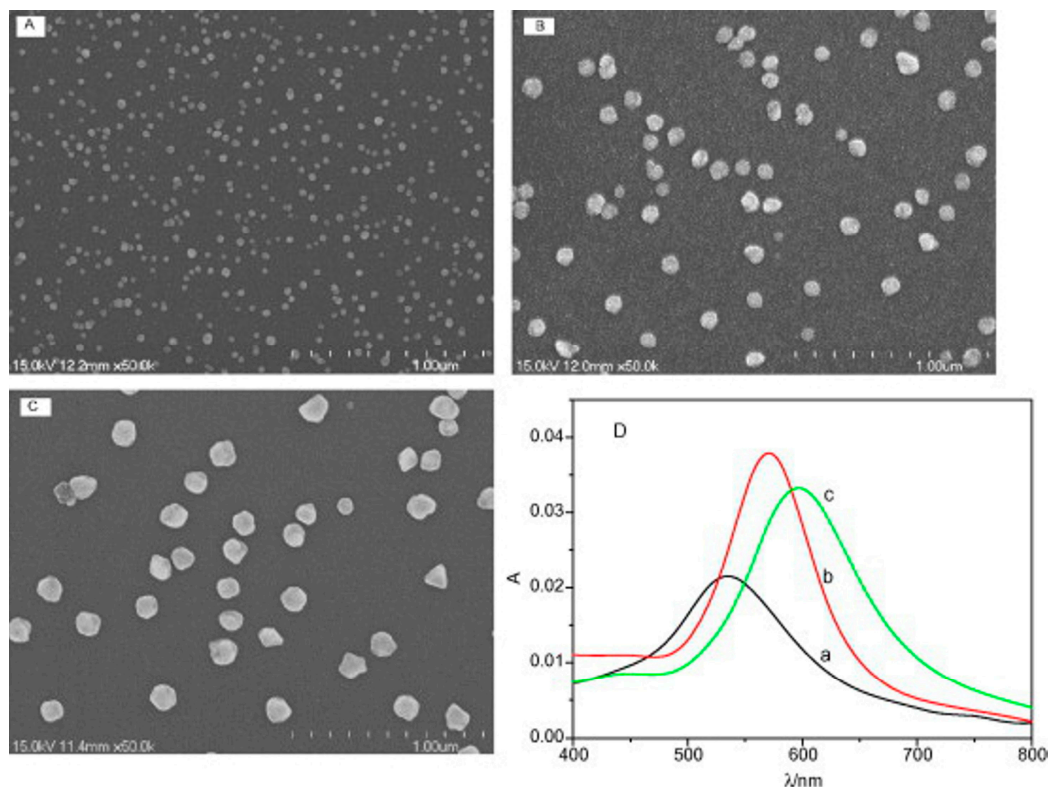


**Figure 2.** Representative SEM images of GNPs (gold nanoparticles) on an indium tin oxide (ITO) surface at an average size of (A) 35 nm, (B) 90 nm, and (C) 130 nm. (D) UV-VIS absorption spectra of the GNPs deposited on an ITO surface. Reproduced with permission from ref. [21], Copyright 2009, Elsevier.

In another example, gold nanoparticles were formed on GCE by sweeping the potential in 10 mM of H<sub>2</sub>AuCl<sub>4</sub> from 1.1 V to −0.1 V (versus Ag/AgCl) for a number of scans ranging from 5 to 35 [22]. The coverage of gold nanoparticles on the surface was observed to increase until a full monolayer of nanoparticles was seen for 25 cycles, and beyond that, multilayers began to form. After 25 cycles, a roughness factor of  $183.6 \pm 1.2$  was determined using [Fe(CN)<sub>6</sub>]<sup>3−/4−</sup> as a diffusing redox probe, with more cycles making the roughness factor drop significantly. A mixed SAM of 4-aminothiophenol (4-A<sub>4</sub>Ph) and 4-mercaptobenzoic acid (4-MBA) was formed. The enzyme *Corynascus thermophilus* cellobiose dehydrogenase, which is the C291Y mutant that was designed for enhanced sensitivity to glucose and lower cross-reactivity with maltose, was immobilized by cross-linking with glutaraldehyde. The result was a selective and stable (over 20 days) third generation (direct electron transfer) biosensor for glucose with a detection limit of 6.2 µM and a linear range from 0.02 to 30 mM. Gold nanoparticles electrodeposited onto GCE were used as a support for a DNA-based electrochemiluminescence (ECL) sensor for Hg<sup>2+</sup> [23]. The Au nanoparticles were electrodeposited for five seconds after a potential step from 1.1 V to −1.0 V (versus Ag/AgCl) in solutions of H<sub>2</sub>AuCl<sub>4</sub> in the range of 40 to 140 µM in 0.5 M of KNO<sub>3</sub>. The surface density of Au nanoparticles increased with the concentration of the H<sub>2</sub>AuCl<sub>4</sub> solution, and the maximal ECL was found when a concentration of 100 µM was used. The distance between ferrocene as a quencher and [Ru(bpy)<sub>3</sub>]<sup>2+</sup> as a reporter would increase greatly upon Hg<sup>2+</sup> binding, which caused the DNA hairpin structure to open up and increased the ECL signal. A detection limit of 0.1 nM for Hg<sup>2+</sup> was found. In another example,

platinum nanoparticles were electrodeposited onto a seven- $\mu\text{m}$  diameter carbon fiber electrode and used as a support for HRP [24]. The Pt nanoparticles were electrodeposited by cycling the potential between 100 mV and  $-250$  mV (versus SCE) at  $15\text{ mV sec}^{-1}$  in  $\text{N}_2$  saturated  $4.7\text{ mM}$  of  $\text{H}_2\text{PtCl}_6$  in  $0.50\text{ M}$  of  $\text{H}_2\text{SO}_4$ . After the deposition of a layer of chitosan, and activation with glutaraldehyde, HRP was immobilized. The direct electron transfer of HRP was observed. A detection limit of  $0.35\text{ }\mu\text{M}$  and a linear range from  $0.64\text{ }\mu\text{M}$  to  $3.6\text{ mM}$  was observed for  $\text{H}_2\text{O}_2$ .

The electrodeposition of gold nanoparticles onto a gold electrode was used to make an RNA aptasensor for cyclic adenosine monophosphate (cAMP) [25]. The gold nanoparticles were electrodeposited by scanning from  $-0.2\text{ V}$  to  $-1.2\text{ V}$  (versus Ag/AgCl) in  $2\text{ mM}$  of  $\text{HAuCl}_4$  in  $0.1\text{ M}$  of KCl. The thiolated RNA aptamer was immobilized, and mercaptohexanol was applied as both a blocker and spacer. Using Faradaic impedance spectroscopy with the  $[\text{Fe}(\text{CN})_6]^{3-/4-}$  redox probe, a limit of detection of  $50\text{ pM}$  for cAMP was achieved. An electrochemical immunosensor for *Salmonella pullorum* was made using gold nanoparticles electrodeposited onto screen-printed carbon electrodes (SPCE) [26]. The nanoparticles were electrodeposited onto SPCE by cycling the potential between  $-1.5\text{ V}$  and  $0.5\text{ V}$  (versus Ag/AgCl) at  $25\text{ mV sec}^{-1}$  in a  $100\text{-}\mu\text{M}$   $\text{HAuCl}_4$ . The surfaces were then modified by the deposition of an anti-*S. pullorum* antibody conjugated to HRP along with an ionic liquid. In the presence of optimized concentrations of  $\text{H}_2\text{O}_2$  and thionine, the current due to enzyme activity was amplified. The reduction in current upon the binding of bacteria to the surface was used as the response, and a detection limit of  $548\text{ CFU mL}^{-1}$  (CFU, colony forming units) was obtained.

Indium tin oxide (ITO)-coated glass is a highly attractive substrate for electrodeposition, as it is optically transparent and useful for sensors based on localized surface plasmon resonance, and is highly versatile, as has recently been reviewed [27]. Gold nanoparticles were electrodeposited onto ITO-coated glass and used as a support for HRP to make an amperometric sensor for  $\text{H}_2\text{O}_2$  [28]. Electrodeposition was carried out by cycling the potential between  $-0.4\text{ V}$  and  $-1.3\text{ V}$  (versus SCE) at  $50\text{ mV sec}^{-1}$  for 20 cycles in a solution of  $2\text{ mM}$  of  $\text{K}[\text{Au}(\text{CN})_2]$  in pH 8 phosphate buffer. SEM (S-4700, Hitachi, Tokyo, Japan) revealed a high coverage of gold nanoparticles of near  $25\text{ nm}$  in size and of low size dispersion. Since the substrate is transparent, absorbance spectroscopy showed the presence of a plasmon absorption peak at  $540\text{ nm}$ . The gold nanoparticles were modified by cysteine, and then, HRP was immobilized by adsorption. Direct electron transfer to the enzyme was observed. The detection limit for  $\text{H}_2\text{O}_2$  was  $2\text{ }\mu\text{M}$ , with a linear range from  $8\text{ }\mu\text{M}$  to  $30\text{ mM}$ . The direct electrodeposition of gold nanoparticles onto an ITO-coated glass electrode was used to make a sensor for morphine [29]. The deposition was done using CV between  $-0.3\text{ V}$  and  $-1.15\text{ V}$  for 60 cycles at  $50\text{ mV sec}^{-1}$  from a solution of  $0.12\text{ M}$  of  $\text{K}[\text{Au}(\text{CN})_2]$  in  $0.02\text{ M}$  of phosphate buffer at  $30 \pm 1\text{ }^\circ\text{C}$ . The nanoparticles formed were  $25$  to  $30\text{ nm}$  and quasi-spherical in shape. Morphine was oxidized readily, and a detection limit of  $0.21\text{ }\mu\text{M}$  and a linear range for  $0.8$  to  $16\text{ }\mu\text{M}$  were found.

Twinned Au nanoparticle structures were formed by electrodeposition onto ITO-coated glass electrodes and used as localized surface plasmon resonance (LSPR) sensors [30]. Deposition to produce twinned structures was done at  $60\text{ }^\circ\text{C}$  and pH 2 by applying 20 cycles from  $0.3\text{ V}$  to  $-0.7\text{ V}$  (versus SCE) at  $50\text{ mV sec}^{-1}$  from  $0.1\text{ mM}$  of  $\text{HAuCl}_4$  and  $0.1\text{ M}$  of KCl. For comparison, isolated Au nanoparticles were electrodeposited onto ITO-coated glass at  $30\text{ }^\circ\text{C}$ . The twinned Au nanoparticles were  $60\text{ nm}$  in size and appeared in chains of two or more with an average aggregation number of 2.3. The twinned Au particles showed two plasmon absorbance peaks at  $540\text{ nm}$  and  $705\text{ nm}$ , which were assigned as longitudinal and transverse, similar to what is seen for gold nanorods [31]. The  $705\text{-nm}$  peak was highly sensitive to refractive index change with a shift of  $245\text{ nm RIU}^{-1}$ . When modified by goat anti-IgG (Immunoglobulin G) monoclonal antibody, the binding of monoclonal IgG from a  $500\text{-ng mL}^{-1}$  solution caused a  $21\text{-nm}$  red shift as compared to only a  $5\text{-nm}$  red shift for isolated Au nanoparticles. Additional study of these twinned structures showed that the longitudinal band emerged at 10 cycles, and grew in prominence at 20 and 40 cycles; the deposition at  $20\text{ }^\circ\text{C}$  did not result in a longitudinal band, and hence no twinned structures; and that the lower potential limit of  $-0.7\text{ V}$  was required for the appearance of the longitudinal band [32]. The size of the particles increased

gradually with the number of deposition cycles, from  $45 \pm 7$ -nm at 10 cycles, and reaching  $80 \pm 8$  nm at 40 cycles.

Gold nanoparticles electrodeposited onto ITO-coated glass electrodes were subsequently coated by a thin silver shell to improve their plasmon absorbance refractive index sensitivity [33]. Gold nanoparticles were electrodeposited by applying 60 cycles in 0.1 mM of  $\text{HAuCl}_4$  at pH 2 between 0.3 V and  $-0.5$  V at  $50 \text{ mV sec}^{-1}$ , and then, a silver shell was electrodeposited by applying 20 cycles between 0–0.3 V in 0.02 mM of  $\text{AgNO}_3$ . The addition of a 0.7-nm silver shell was optimal for increasing the refractive index sensitivity of the structure, and resulted in a five-nm blue-shift in the absorbance peak. The average size of the deposited Au particles increased from  $72 \pm 12$  nm to  $89 \pm 13$  nm if 200 cycles of Ag deposition were applied. The complimentary approach of electrodepositing Ag nanoparticles onto ITO glass and then electrodepositing a 1.3-nm gold shell also enhanced the plasmon absorbance refractive index response, from 123 nm  $\text{RIU}^{-1}$  for Ag nanoparticles to 230 nm  $\text{RIU}^{-1}$  for the silver nanoparticles covered with a gold shell [34]. When Au nanoparticles were electrodeposited onto ITO glassware, it was found that the larger ones with an average size of 130 nm had the highest plasmon absorbance peak wavelength response to a refractive index change of 187 nm  $\text{RIU}^{-1}$  [21]. The plasmon absorbance peak red shifted with increasing nanoparticle size, which was controlled by varying the number of cycles of potential between 0.3 V and  $-0.5$  V (versus SCE) from 10 to 20 to 40 cycles at  $50 \text{ mV sec}^{-1}$ . Cyclic voltammetry as an electrodeposition method was noted as superior to single potential step methods for controlling nucleation and growth rates.

Au nanoparticles electrodeposited on ITO glass were found to show the electrocatalytic oxidation of glucose [35]. The deposition was carried out from 0.12 mM of  $\text{K[Au(CN)}_2\text{]}$  in 0.05 M of pH 7.4 phosphate buffer by cycling the potential from  $-0.3$  V to lower limits of either  $-1.15$  V,  $-1.20$  V, or  $-1.25$  V (versus SCE) at  $50 \text{ mV sec}^{-1}$ . The particle size increased with a more negative lower limit, from 20 to 30 nm at  $-1.15$  V to 35 to 45 nm at  $-1.20$  V and to 50 to 60 nm at  $-1.25$  V. A linear range of 0.004 to 0.50 mM for glucose was achieved in 0.01 M of NaOH when the applied potential was 0 V.

### 2.3. Constant Current Deposition

Electrodeposition at either a fixed potential or during potential cycling are the two most widely reported approaches, but constant current approaches have also been reported. Gold nanoparticles deposited under conditions of fixed current density were prepared [36]. Electrodeposition was performed onto ITO-coated glass electrodes from 2 mM of  $\text{HAuCl}_4$  in 0.2 M of HCl. At a current density of  $11 \text{ mA cm}^{-2}$ , smaller nanoparticles near 14 nm were obtained, but lowering the current density to  $5.92 \text{ mA cm}^{-2}$  gave larger nanoparticles near 18 nm. Increasing the total charge passed increased the surface density of the nanoparticles. Electrocatalytic activity toward the oxidation of ascorbic acid was observed. Platinum containing zinc oxide nanospheres were electrodeposited onto GCE from a solution of 0.01 M of  $\text{ZnO}_3$ , 0.01 M of hexamethylenetetramine, and 0.01 M of  $\text{H}_2\text{PtCl}_6$  at 1 V (versus  $\text{Hg/Hg}_2\text{SO}_4$ ) and  $7.073 \text{ mA cm}^{-2}$  current for one hour [37]. The atomic percentage of Pt in the structures was 2%. The electrodeposited structures showed separate 10 to 200-nm spherical agglomerates on the surface of the first one and the overall diameter was 0.2 to 3.5  $\mu\text{m}$ . Cholesterol oxidase was physisorbed onto these structures to make an amperometric cholesterol biosensor based on the detection of  $\text{H}_2\text{O}_2$  at +0.2 V. The sensor had a linear range of 0.5 to 15  $\mu\text{M}$  of cholesterol, with a maximum response at pH 6.8 and near 60 °C, and retaining 95% activity after storage for 30 days.

### 2.4. Electrostatic Deposition

In some studies, the gold nanoparticles are prepared first, and then electrodeposited onto the surface, with the applied potential promoting nanoparticle binding to the surface. For example, one study reported the solution phase preparation of gold nanoparticles (average size = 31.9 nm as determined by dynamic light scattering) by citrate reduction followed by their electrodeposition using a combination of chronopotentiometry and CV [38]. In the reported process, chronopotentiometry was used to vary the potential (versus  $\text{Ag/AgCl}$ ) from 2.5 V to 0.2 V over 60 s followed by 90 cycles between



−0.2 V and 0.8 V at 50 mV sec<sup>−1</sup>. Scanning electron microscopy showed that the gold nanoparticles were distributed on the surface as mostly uniform areas, but there were also some non-uniform areas. The gold surfaces were then modified by SAMs of 11-mercaptoundecanoic acid, to which aptamers were conjugated using EDC/NHS coupling chemistry. The aptamers were specific to HCT116 colon cancer cells expressing carcinoembryonic antigen. A detection limit of six cancer cells mL<sup>−1</sup> was achieved by measuring the suppression of the redox current of the [Fe(CN)<sub>6</sub>]<sup>3−/4−</sup> redox probe upon cell binding, and this response was linear up to 25 cancer cells mL<sup>−1</sup>.

### 3. Biosensor Application of Nanostructures Electrodeposited onto a Template

Electrodeposition onto templates can produce uniquely regular nanostructures, either as interconnected morphologies or as regular patterns of unique shapes. Some of the templates that have been used to date include thin deposited films of colloidal particles that pack in a regular lattice or array, such as polystyrene spheres or silica spheres, and anodic aluminum oxide membranes that present an array of pores, masks, and templates specially prepared using photolithography. In principle, variation of the template dimensions can be used to precisely vary the dimensions of the resulting nanostructure and open up more possibilities for optimizing the analytical performance of the resulting biosensor.

#### 3.1. Electrodeposition onto Regularly Packed Thin Films of Colloidal or Nanoscale Spheres

A popular and low-cost means of preparing an ordered template is the assembly of spherical colloidal particles of polystyrene or silica into hexagonal close-packed arrays. Such arrays can vary in the number of layers deposited on a substrate, and these layers can be produced by methods including vertical deposition, spin coating, and dip coating [39]. The degree of order in these arrays can be high, extending over centimeters with occasional defects. Following electrodeposition into the interstices between the particles, the template of spheres can be dissolved and washed away using solvent. The resulting macroporous metal structure has been achieved for gold and platinum [40] and also for platinum, palladium, and cobalt [41]. The polystyrene spheres are produced by emulsion polymerization, and are commercially available in a range of sizes. Through the colloidal template approach, the surface area of the electrode and its morphology can be controlled in a systematic way by varying the colloidal particle size, film thickness, and electrodeposition parameters. Then, such an approach allows for clearer study of the relationship between electrode structure and biosensor performance.

Macroporous platinum films were formed by electrodeposition onto a self-assembled layer of polystyrene spheres, which is then followed by the use of solvent to remove the spheres [42]. A silicon wafer covered by a 200-nm layer of gold over a five-nm chromium adhesion layer was prepared by thermal evaporation. Polystyrene spheres of 460-nm diameter were carefully spread over a water–air interface, and then transferred by dip coating, with repeated transfers to build up multiple layers of close-packed spheres. Then, electrodeposition was carried out by cycling the potential from −0.18 V to 1.20 V (versus Ag/AgCl) at 175 mV sec<sup>−1</sup> in a solution of five mM of H<sub>2</sub>PtCl<sub>6</sub>, 0.2 M of H<sub>2</sub>SO<sub>4</sub>, and 35 mM of polyvinylpyrrolidone, which served to promote a uniformity of deposition. After deposition, the template of polystyrene spheres was removed by Soxhlet extraction in toluene. The amount of Pt that was electrodeposited was used to define layers; for example, it was a ‘three-fourths deposit’ if the platinum was as high off the surface as three-fourths of the diameter of a polystyrene sphere or a seven-fourths deposit if the platinum was as high as 1.75 times the diameter of a Pt sphere. The first layer of the structure showed interconnected pores, and the second layer had pores connected to the first layer, which allowed for both horizontal and vertical fluid penetration. Using an underpotential deposition of H<sub>2</sub>, a roughness factor of 30.3 ± 1.0 was determined for the seven-fourths deposit. Figure 3 shows SEM (Strata DB235, FEI Co., Hillsboro, OR, USA) images of one-third, three-fourths, and seven-fourths deposits, along with an optical micrograph of an electrode. For these structures, the roughness factor as measured electrochemically steadily increased, being 18.3, 24.9, and 30.3, respectively.

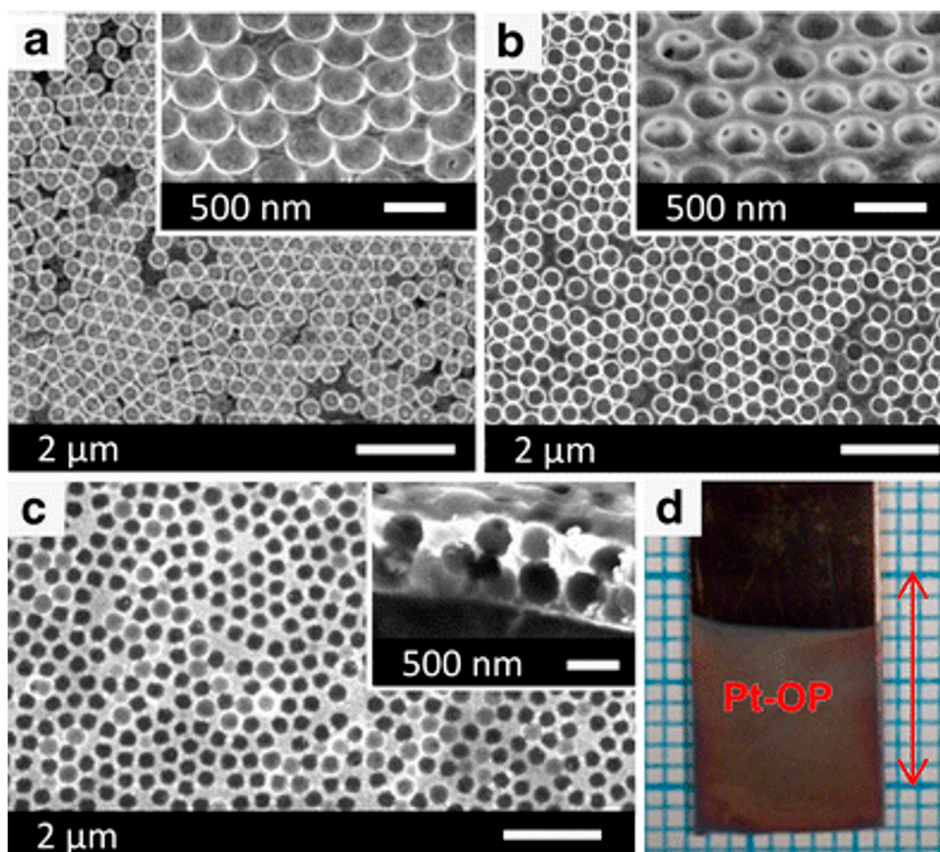


**Figure 3.** Scanning electron microscopy (SEM) images of representative samples for each type of Pt-OP (platinum ordered porous) electrode: (a) sample type one-third (inset, viewed at a 45° tilt); (b) sample type three-fourths (inset, viewed at a 45° tilt); and (c) sample type one and three-fourths (inset, cross section viewed at a 60° tilt). (d) Optical micrograph of a typical Pt-OP electrode with a length of one cm indicated by the arrow on the grid. Reproduced with permission from ref. [42], Copyright 2013, Elsevier.

Electrodeposition onto a template was used to create a surface-enhanced Raman active (SERS) substrate [43]. ITO-coated glass was used as support for a 10-nm layer of sputter-coated gold. A monolayer of two- $\mu\text{m}$  diameter polystyrene spheres was formed on another glass slide, and then transferred onto the gold-coated ITO, which was then used as the substrate for electrodeposition from  $0.5 \text{ g L}^{-1}$  of  $\text{HAuCl}_4$  solution at a constant current of  $0.04 \text{ mA cm}^{-2}$  for various fixed times from two to 30 h. Then, the polystyrene spheres were washed away using methylene chloride, leaving behind a hierarchical structure of the array of indentations previously occupied by the microspheres and electrodeposited gold structures resembling aggregated nanorods in what had been the gaps between the microspheres. The Raman intensity for adsorbed rhodamine 6G measured at  $1362 \text{ cm}^{-1}$  was high for structures prepared by electrodeposition for five–fifteen hours, but significantly lower on those prepared for either 30 h or two hours. The approach taken in this study allowed for comparison of the produced template versus non-templated structures, and showed superior signal intensity for the structures produced on the template, which was further improved by optimizing the electrodeposition time.

The electrodeposition of Au nanoparticles onto a template of three-dimensional close-packed silica spheres of 320-nm diameter was used to create an ordered macroporous structure of connected Au nanoparticles [44]. Producing such a structure was noted as having the advantage of providing both a high surface area and a high conductivity. The silica spheres were deposited on gold-coated glass slides by a vertical dipping method. Au nanoparticles were electrodeposited from 5.0 mM of  $\text{HAuCl}_4$  by first allowing one hour of immersion, and then applying 0.5 V (versus SCE) until a desired amount

of charge was passed, such as 0.1 C. The silica spheres were removed using aqueous hydrofluoric acid (HF). The remaining structure resulted from the deposition of gold nanoparticles that were found to have an average size of 4.09 nm in the interstices between the silica spheres, and was macroporous and interconnected as a framework. Hemoglobin was adsorbed onto the structure over times up to three hours. Using electrochemical impedance spectroscopy with the  $[\text{Fe}(\text{CN})_6]^{3-/4-}$  redox probe, a coverage of 88% was determined for the protein. Coverage of the gold surface by protein significantly reduced the capacitance and also decreased the charge transfer rate constant of the redox probe. Direct electron transfer between the Au nanoparticles of the framework and hemoglobin was observed, and using the Laviron analysis [45], an electron transfer rate constant of  $0.95 \text{ sec}^{-1}$  was obtained.

Nanorings and split nanorings of a range of metals were formed by electrodeposition onto a special template using a process referred to as lithographically-patterned nanoscale electrodeposition [46]. Gold nanorings produced by nanosphere lithography using vapor deposition were found to have a superior refractive index response of  $350 \text{ nm RIU}^{-1}$  with a high figure of merit of 3.1, and were found to give excellent performance as real-time sensors for DNA hybridization [47]. Hence, there is a significant value to producing nanorings by the more straightforward approach of electrodeposition. Split nanorings exhibit independently addressable plasmonic resonances, depending upon the polarization of the incident light, and thus have attracted interest for use in multiplexed DNA sensing [48]. A monolayer of polystyrene beads was first spin-coated onto hydrophilic glass slides, and then etched in oxygen plasma to reduce their size. Then, a 70-nm layer of silver was thermally evaporated over the beads, and the beads were removed by sonication in toluene and then in acetone. Positive photoresist was spin-coated over this nanohole array. To ultimately make nanorings, the photoresist was backside exposed at normal incidence, or backside exposed at a variable angle to produce split nanorings. Holes form in the photoresist upon development, and through those holes, a range of metals were electrodeposited to produce nanorings or split nanorings, including nickel, cobalt, cadmium selenide, and gold. The gap in the split nanorings increased with the increase in the angle of backside exposure. The gold nanorings and split nanorings showed plasmonic absorbance in the near-infrared tunable over a wide range that could potentially be applied to biosensor development. Nanoring arrays were formed using this approach, for which the ring width and outer radius were varied [49]. When the outer radius increased from 285 to 400 nm, and the ring width was kept in the range of 125 to 155 nm, the plasmon resonance peak in the near infrared increased linearly with the increasing outer diameter. The plasmon absorbance was tunable for nanorings made of gold, silver, or nickel. Figure 4 shows SEM (Magellan, FEI Co., Hillsboro, OR, USA) images of gold nanorings, which were created using one- $\mu\text{m}$  colloids.

### 3.2. Electrodeposition through Aluminum Oxide and other Templates

Aluminum anodized in polyprotic acid will generate aluminum oxide with pores parallel to the surface whose diameter depends on the applied voltage and can range from 10 to 450 nm [50]. Each pore is part of a hexagonal domain of aluminum oxide [51]. The mechanism of pore formation has been described, and involves breaking Al–O bonds and the release of  $\text{Al}^{3+}$  [52]. Gold nanotube arrays or gold nanowire arrays were formed by galvanostatic (current controlled) electrodeposition into an anodic aluminum oxide template with a 200-nm pore size and applied to non-enzymatic glucose sensing [53]. The aluminum oxide templates were sputter coated with a 300-nm thick gold layer. Electrodeposition was carried out at a constant current of  $0.1 \text{ mA cm}^{-2}$  in an electroplating bath containing  $\text{HAuCl}_4$ ,  $\text{Na}_2\text{SO}_3$ , ethylenediaminetetraacetic acid (EDTA),  $\text{K}_2\text{HPO}_4$ , and  $\text{CoSO}_4$ . Electrodeposition at pH 9 resulted in nanowires that were two  $\mu\text{m}$  in length, but adjustment to pH 11 using KOH resulted in the formation of nanotubes with 50-nm openings. After etching away the aluminum oxide template, the arrays were affixed to a GCE using Nafion. The gold nanotube arrays when used at 0.25 V gave higher sensitivity than the nanowire arrays for glucose oxidation, and achieved a detection limit of  $2.1 \mu\text{M}$  and a linear range from five  $\mu\text{M}$  to 16.4 mM. In contrast, the nanowire arrays gave a detection limit of  $12.8 \mu\text{M}$  and a linear range from 20  $\mu\text{M}$  to 15.2 mM.

The authors noted that the nanotube arrays had a higher active surface area than the nanowire arrays by a factor of almost two. The approach of electrodeposition onto aluminum oxide templates can in principle allow for variation in nanowire or nanotube size, since the pore diameter and spacing in this type of template can be varied during its preparation.

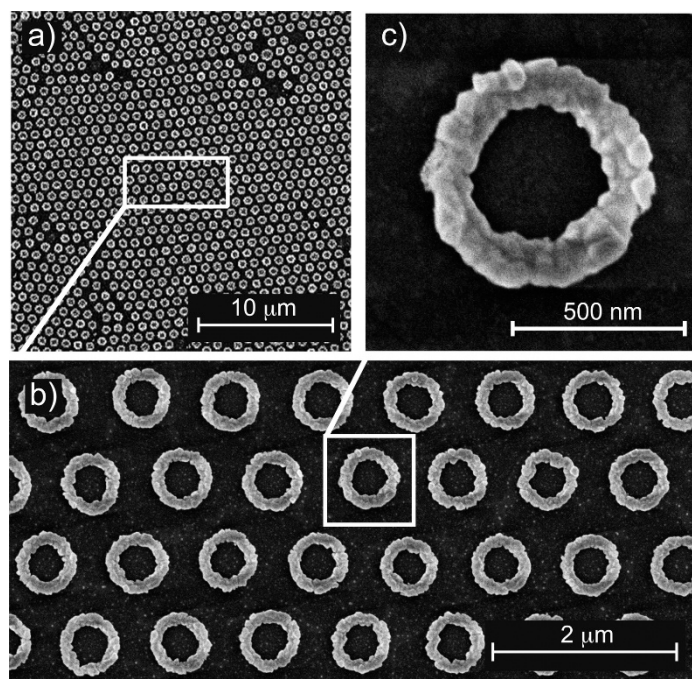


**Figure 4.** SEM images of Au nanorings created from one- $\mu\text{m}$  colloids. (a) Low magnification image of a domain of ordered nanorings. (b) Increased magnification of nanorings with outer radius =  $330 \pm 5$  nm and width =  $135 \pm 4$  nm, and (c) the highest magnification of a single ring. Reproduced with permission from ref. [49], Copyright 2013, American Chemical Society.

Electrodeposition was used to create gold nanowire arrays as a support for an enzymatic glucose sensor in a flow-injection system [54]. Anodic aluminum oxide templates with a thickness of  $16 \mu\text{m}$  and  $80\text{-nm}$  pores were used as templates. The gold wire nanoarrays were fixed onto a three-mm diameter gold electrode using conductive carbon tape. The enzymes glucose oxidase and HRP were cross-linked on the gold surfaces in the presence of bovine serum albumin (BSA). The composition of enzymes and of BSA was optimized along with the pump time and sampling speed. The optimal working potential was found to be  $0.05 \text{ V}$  (versus  $\text{Ag}/\text{AgCl}$ ), and a detection limit of one  $\mu\text{M}$  was achieved with a linear range from five to  $1000 \mu\text{M}$ . The response of the electrode declined only 4% over 10 days, and 93% of the response remained after the determination of 40 samples. The regular spacing and uniformity of size of the nanowires provided a structure into which the cross-linked enzymes and proteins could become coated between and around the nanowires, as can be seen in Figure 5, which shows the nanowire array before and after protein modification. The author pointed out the distinct advantage of this arrangement for facilitating electron transfer between the nanowires and the active enzyme sites.

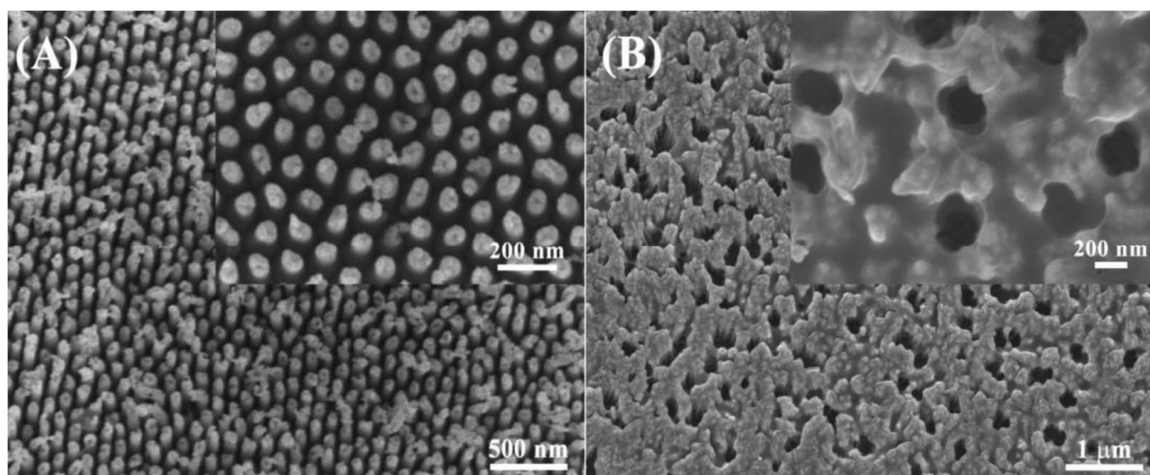


**Figure 5.** Top-view of the SEM images of Au NWAs (gold nanowire arrays) without modification (A) and modified with GLA-BSA-GOx-HRP (GLA = glutaraldehyde, BSA = bovine serum albumin, GOx = glucose oxidase, HRP = horseradish peroxidase) (B). Reproduced with permission from ref. [54], Copyright 2014, Electrochemical Society.

A highly ordered array of Pt nanotubules was produced by electrodeposition into a porous anodic alumina template, and found to be effective as a non-enzymatic glucose sensor [55]. The porous alumina membrane was first modified with 3-aminopropyltrimethoxysilane, and then Pt was electrodeposited from 8.23 mM of  $K_2PtCl_6$  in 30 g L<sup>-1</sup> of boric acid at -0.1 V (versus SCE) until a desired amount of charge had passed. Immersion in 3 M of NaOH removed the alumina template and left behind Pt nanotubules that were three  $\mu\text{m}$  in length, had a  $70 \pm 10$ -nm inner diameter and had a  $150 \pm 10$ -nm outer diameter. The roughness factor of the surface was found to be 758. The amperometric detection of glucose at 0.4 V gave a detection limit of 1.0  $\mu\text{M}$  and a linear range from two to 14 mM.

The electrodeposition of Au through an alumina nanomask covering an ITO-coated glass surface was used to create an ensemble of hemispherical gold nanoparticles [56]. The alumina mask was prepared by the chemical solution deposition of block copolymer and aluminum chloride followed by drying and heating [57]. The holes in the nanomask were 8.6-nm deep and 34-nm in diameter, and their surface density was 300  $\mu\text{m}^{-2}$ . Electrodeposition was carried out at -0.5 V (versus Ag/AgCl) for 10 s. The nanomask allowed improved control of nanoparticle size and inter-particle spacing. It was also noted that the use of the nanomask improved the thermal stability of the ensemble of particles, preventing coalescence at temperatures as high as 500 °C. The nanoparticles showed a plasmon absorbance peak at 559 nm in air that red shifted when exposed to liquid media of higher refractive index, which indicated that the nanoparticles were useful for application as localized surface plasmon resonance biosensors.

Gold nanotube arrays were also prepared by electrodeposition to make a biosensor for detecting DNA from mycobacterium tuberculosis [58]. A polycarbonate membrane with 200-nm pores was sputter coated on one side with a gold layer. Subsequently, Au was electrodeposited inside the membrane at -1.0 V (versus Ag/AgCl) from a gold plating solution. The average length of the supported vertical nanotubes was 1.5  $\mu\text{m}$ , and they were 200 nm in diameter. The authors noted that nanotube arrays produced by electrodeposition are less prone to deformation or bunching of nanotubes as compared to those produced by physical or chemical vapor deposition. The gold-coated membrane was then placed on a gold electrode using conducting paste, and an O-ring was used to position the electrochemical cell. The polycarbonate template was dissolved using dichloromethane. A thiolated probe DNA sequence was immobilized on the gold surface. Detection of the complimentary DNA strand from the bacteria was achieved using the methylene blue redox probe and DPV. A detection limit of 0.05 ng  $\mu\text{L}^{-1}$  was obtained. The same authors had previously demonstrated the application of

similarly prepared gold nanowire arrays in the electrochemical detection of DNA hybridization [59]. Figure 6 shows a schematic of the process that was used to create these gold nanotube array sensors. In related work [60], a sensor for DNA from human papillomavirus (HPV) was developed by electrodeposition onto polycarbonate membranes also presenting pores in the 150 to 200-nm size range, randomly arranged. The inner pores were surface modified with 3-aminopropyltrimethoxysilane. A 20-nm layer of gold was sputter coated onto one side of the template, and short nickel nanotubes were electrodeposited at  $-900$  mV (versus Ag/AgCl) from a solution containing  $0.8$  M of  $\text{NiSO}_4$  in  $0.3$  M of  $\text{H}_3\text{BO}_3$ . The short nickel nanotubes served to protect the backside of the membrane. Gold nanotubes with edge thicknesses of 30 to 50 nm and 100 nm in average diameter were formed by electrodeposition from  $10$  mM of  $\text{KAu}(\text{CN})_2$  at  $-1400$  mV for 300 s. Then, the polycarbonate template was partially dissolved in  $\text{CH}_2\text{Cl}_2$ . The gold surfaces were modified by a thiolated capture oligonucleotide. The detection of the target HPV oligonucleotide was carried out using electrochemical impedance spectroscopy (EIS), measuring the change in charge transfer resistance as a function of target DNA concentration in two mM of  $\text{K}_4[\text{Fe}(\text{CN})_6]$  +  $2$  mM  $\text{K}_3[\text{Fe}(\text{CN})_6]$  at the open circuit potential and using a  $10$ -mV potential modulation over the range from  $0.01$  Hz to  $100$  KHz. The new and novel feature of the study was that EIS was carried out in the presence of an externally applied and separate applied electric field of  $+5$ V. It was found that the application of an external field, which promoted the DNA probe to lay flat on the gold surface, greatly increased the sensitivity of the charge transfer resistance to target DNA binding. Sensitivity for the target DNA of one fM was achieved, which was lower than all except one other report for the same target, and a good linear range from  $0.01$  pM to  $1$   $\mu\text{M}$ .

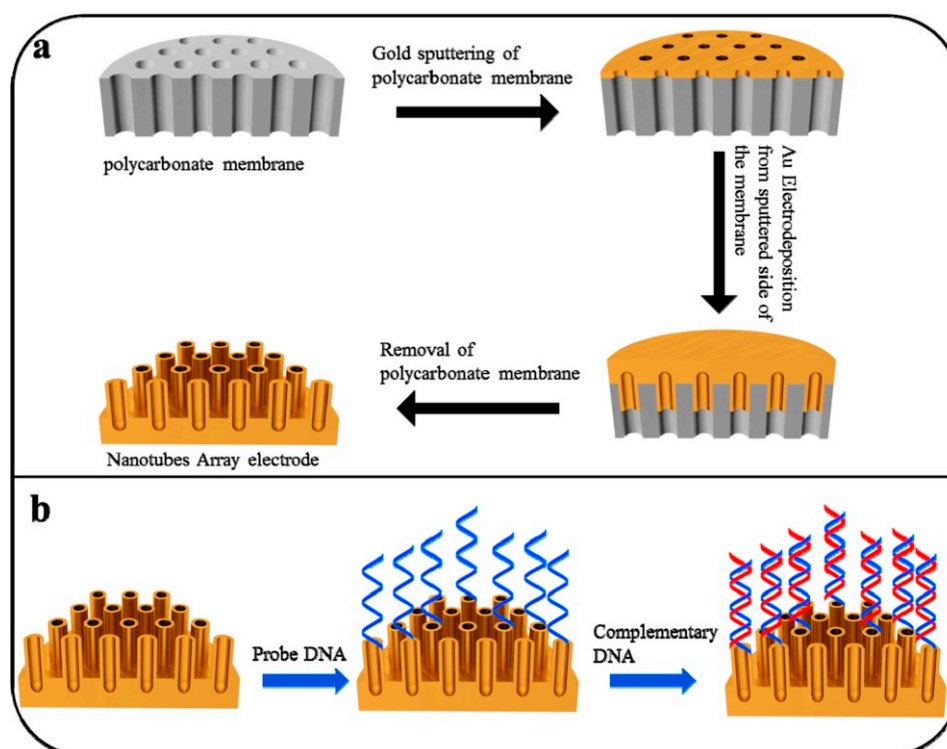


**Figure 6.** Schematic drawing of (a) synthesis of AuNTsA (Gold nanotubes array) and (b) fabrication of the DNA hybridization biosensor based on AuNTsA electrodes. (WE–working electrode, RE–reference electrode, CE–counter electrode). Reproduced with permission from ref. [58], Copyright 2016, Elsevier.

### 3.3. Other Templates for Electrodeposition

The electrodeposition of palladium inside a nanoporous gold (np-Au) electrode was used to create an electrochemical biosensor for the neurotransmitter dopamine [61]. Nanoporous gold provides an

interconnected and continuous structure of high conductivity. The np-Au covered a 0.2-mm diameter gold wire electrode with inter-ligament gaps of about 200 nm, and was then placed in a solution of five mM of sodium dodecyl sulfate and 2.5 mM of PdCl<sub>2</sub>, and the potential was cycled between 0.2 V and 1.2 V (versus SCE) to form a near 20-nm thick Pd coating inside the np-Au. The np-Au/Pd electrode was found to be sensitive to dopamine oxidation as detected using differential pulse voltammetry with a resulting sensitivity of 1.19 μA μM<sup>-1</sup>, a detection limit of one μM, and a detection range of one to 220 μM. The electrode was found to be stable for up to 40 repetitions of use, and the dopamine signal was not affected significantly by potential interferents such as ascorbic acid, uric acid, and others.

A complex nanostructured zinc oxide electrode coating based on a phospholipid template was used to incorporate the enzymes alcohol dehydrogenase or glucose oxidase to make amperometric sensors for ethanol or glucose operating with direct electron transfer [62]. The phospholipid 1,2-dipalmitoyl-sn-glycero-3-phosphate (DPGP) was used to form lamellar bilayer structures for templating the formation of lamellar mesoporous ZnO upon electrodeposition. DPGP at 0.02 wt% was dissolved in 25 wt% of N-methyl-2-pyrrolidone (NMPD). Electrodeposition was carried out from the 0.02-M Zn(NO<sub>3</sub>)<sub>2</sub> solution with DPGP and NMPD, and also in the presence of enzyme at a four to one weight ratio of DPGP/enzyme at -0.5 V (versus SCE) for 60 min onto gold plates. Electrodeposition without enzyme resulted in a morphology of cross-linked flakes under SEM (S-4800, Hitachi, Tokyo, Japan). Higher magnification transmission electron microscopy (TEM) (Tecnai G2 F20 S-Twin, FEI Co., Hillsboro, OR, USA) showed that the flakes were lamellar stacks with a 0.436-nm repeat distance. X-ray diffraction confirmed a 0.437-nm repeating lamellar phase of ZnO formed between DPGP bilayers. Upon the addition of enzyme, the film changed to a smoother flat morphology, for a 200-nm thick film, and TEM revealed arrays of 2.5 to 3.5-nm nanopores. The use of a lipid template was proposed for providing a biocompatible environment, allowing successful electrodeposition with protein. The enzyme-incorporating films showed a high level of direct electron transfer. For ethanol, a detection limit of 2.1 μM was found, and for glucose, the detection limit was 3.6 μM.

Diatoms, the silica shell of microalgae, were electrodeposited together with gold onto screen-printed carbon electrodes at a range of potential, time, and HAuCl<sub>4</sub> concentration [63]. Diatoms and other biominerals provide inorganic templates that already present porous microstructures requiring no complex fabrication. Dendritic gold microstructures were observed on deposition at -1.0 V, but when electrodeposition was carried out at -0.5 V, mostly 15 to 20-μm gold microspheres were observed. If the HAuCl<sub>4</sub> concentration was lowered from 0.60 M to 0.15 M and electrodeposition carried out at -0.5 V, leafy morphologies were seen. The diatoms were immobilized intact and mixed in with the gold microstructures. The modified electrode was found to be electrocatalytically active for the oxidation of H<sub>2</sub>O<sub>2</sub>. The modified electrode was also used as a support for an immunoassay against the toxin microcystin, which is found in drinking water, with an immobilized antibody and HRP-labeled microcystin used for the assay. A recent study used coccoliths, which are biomineral shells isolated from *Emiliania huxleyi*, a photosynthetic bacterium, as templates for the electrodeposition of gold to make an aptamer-based sensor for vaspin, a 42.5-kDa adipose tissue-derived serine protease inhibitor [64]. The coccoliths were about four μm in size, with many pores able to provide an increased surface area. The coccoliths were drop cast onto screen-printed gold electrodes, sputter coated with gold, and the gold was electrodeposited at -1.2 V (versus Ag) from an HAuCl<sub>4</sub> solution (concentration not given) for 70 s to create a roughened surface. The gold surfaces were modified with a first thiolated aptamer that would bind vaspin; then, a second aptamer would bind from solution to create a sandwich structure of vaspin between the two aptamers. The reduction in chronoamperometric current from five mM of K<sub>3</sub>[Fe(CN)<sub>6</sub>] with vaspin concentration in human serum was used to determine a limit of detection of 2.58 nM for the electrodes modified first with the coccoliths. Without the increase in surface area provided by the coccoliths, a limit of detection of 7.72 nM was found.

#### 4. Biosensor Application of Ramified or Dendritic Electrodeposited Structures

Dendritic structures that can form during crystallization from solution or electrodeposition form on the basis of fast growth along one axis, which represents an energetically favorable crystallographic face. The dendritic structures that often emerge under conditions of a stronger driving force for deposition such as a more negative potential may require the addition of a structure-directing agent that favorably adsorbs on a particular crystal face. In the case of gold surfaces, amine-containing compounds would be frequent choices. Other observed morphologies have been classified as ‘fractal’, which is meant to imply morphological self-similarity on multiple length scales [65]. The rapid growth and advancement of an interface can lead to interfacial instability [66], and hence, the emergence of ramified or irregular morphologies such as those referred to as ‘flower-like’. Electrodeposition has been modeled theoretically [67], and has been the subject of computer simulations [68]. Ramified or dendritic nanostructures provide an increased surface-to-volume ratio when particles of the same volume of material are compared. The surfaces of such nanostructures will have regions or directions of greater curvature that may allow larger molecules to pack in a less crowded manner, making terminal functional groups or binding sites more accessible. For example, the deflection angle between neighboring oligonucleotides has been calculated to be greater for small particles of greater curvature [69]. Ramified or dendritic nanostructures will project further out into solution, such that biomolecules may be more effectively presented for interaction with their binding partners or substrates. Dendritic structures present a different distribution of crystal faces, and in the case of gold, the Au (111) face is favored along the growth axis, and present in the structure to a greater extent than for spherical gold nanoparticles [70].

##### 4.1. Dendritic-Like Nanostructures

The electrodeposition of ‘ice-like’, dendritic gold nanostructures on a gold electrode was used to construct a DNA sensor for an *Enterococcus faecalis* gene sequence [71]. Electrodeposition was carried out at 0.0 V (versus Ag/AgCl) for 300 s in a solution of 0.5 M of H<sub>2</sub>SO<sub>4</sub>, 0.020 M of HAuCl<sub>4</sub>, and 0.150 M of sorbitol. The fractal dimension of the nanostructures of  $2.44 \pm 0.19$  was obtained by analysis of the SEM (Mira 3-XMU, TESCAN, Brno–Kohoutovice, Czech Republic) images, and a roughness factor of 9.5 was found. Thiolated DNA was immobilized onto the Au nanostructures, and pinholes were filled using 6-mercapto-1-hexanol. The binding of the complimentary DNA strand, which was released from the bacteria, was detected using DPV scans with toluidine blue as the redox probe, and the higher binding affinity of redox probe for double-stranded DNA (dsDNA) over single-stranded DNA (ssDNA). A limit of detection for the complimentary DNA strand of  $4.7 \times 10^{-20}$  mol L<sup>-1</sup> that was 25 nucleotides long was found with a range of detection from  $1.0 \times 10^{-17}$  to  $1.0 \times 10^{-10}$  mol L<sup>-1</sup>.

The rapid and convenient preparation of dendritic gold nanostructures onto fluorine-doped tin oxide (FTO)-coated glass was achieved from a solution of HAuCl<sub>4</sub> containing 0.1 vol% of 3-aminopropyltriethoxysilane (3-APTS) as a structure-directing agent [72]. Electrodeposition was carried out at -0.25 V (versus Ag/AgCl) for 300 s. 3-APTS forms a moderately strong bond to the Au surface, preferring the Au(111) plane, and induces anisotropic growth and the formation of dendrites that were not observed in its absence. The structures exhibited an electrocatalytic oxidation of glucose and of H<sub>2</sub>O<sub>2</sub>.

Hyperbranched pine-like gold nanostructures were prepared on the surface of a gold electrode by electrodeposition in a solution of 20 mM of HAuCl<sub>4</sub>, 0.5 M of H<sub>2</sub>SO<sub>4</sub>, and 150 mM of histidine, serving as a structure-directing agent [73]. Electrodeposition was at 0.0 V (versus Ag/AgCl) for 600 s. The hyperbranched pine-like and dendritic morphology appeared to be composed of nanoparticles that were 150 to 200 nm in size. Electrochemical determination of the real surface area using the [Fe(CN)<sub>6</sub>]<sup>3-/4-</sup> redox probe and the Randles–Sevcik equation gave a roughness factor of 8.2. The resulting electrode was found to be effective as a non-enzymatic sensor for glucose at a potential of 70 mV, and had a limit of detection of 3.39 μM, and a linear range from 0.020 mM to 0.240 mM. The sensor showed good selectivity against a range of interferents, including theophylline, lysine,



methionine, histidine, xanthine, arginine, and ascorbic acid. The operating potential of 70 mV was lower than others that had been reported.

Electrodeposited gold microstructures with nanoscale dendritic morphology were used as a sensor for a glycoprotein HRP based on the carbohydrate–boronic acid interaction [74]. Electrodeposition from 0.1 M of  $\text{Na}_2\text{SO}_4$  and 30 mM of  $\text{HAuCl}_4$  at  $-0.6$  V (versus Ag/AgCl) for 400 s onto a gold electrode produced dendritic forms that were microns in size, with dendritic morphology on the nanoscale. The gold surfaces were modified with 4-mercaptophenylboronic acid. The interaction of the boronic acid with cis-diols such as those found in the glycans on the glycoprotein resulted in the formation of cyclic esters, thus binding the glycoprotein to the surface. The glycoprotein binding reduced the current for gold oxidation near 1.2 V. A detection limit of 0.5 nM and a linear range from 2.5 nM to 25 mM was obtained using the reduction in the peak current for gold oxidation as the sensing response.

Nickel hydroxide-covered copper dendrites were formed on a gold electrode surface and used as a non-enzymatic glucose sensor [75]. The copper dendrites were formed by electrodeposition from 0.15 M of  $\text{CuCl}_2$  and 0.75 M of  $\text{H}_2\text{SO}_4$  at  $-0.5$  V (versus Ag/AgCl) for five minutes. The primary stems of the dendrite were 10  $\mu\text{m}$  in length with branches 0.1 to 2.0  $\mu\text{m}$  in length and 0.3  $\mu\text{m}$  in diameter. Nickel hydroxide was deposited using chronopotentiometry at a current of  $-0.1$   $\text{mA cm}^{-2}$  in a solution of 0.1 M of  $\text{Ni}(\text{NO}_3)_2$  and 0.1 M of  $\text{KNO}_3$  for 10 min. Glucose detection was carried out at a potential of 0.6 V in 0.1 M of NaOH. A detection limit of 0.24  $\mu\text{M}$  and a linear range from one  $\mu\text{M}$  to 4.5 mM were obtained, and the analysis both worked well for glucose spiked into human urine samples, and was resistant to interferents such as urea, aspartic acid, ascorbic acid, dopamine, and uric acid.

Dendritic gold nanostructures formed by electrodeposition were used as the basis of a sensor for superoxide [76]. At a constant current of  $-1.0$  mA and for fixed times of either 300 s, 500 s, or 700 s, gold was electrodeposited onto a GCE from a solution of five mM of  $\text{HAuCl}_4$  in one M of  $\text{H}_2\text{SO}_4$ . For a 700-second deposition, the surface was covered with dendritic gold structures. Using the gold oxide stripping method, the surface area of  $2.21 \pm 0.01$   $\text{cm}^2$  was found, which was 31.6 times greater than the geometric surface area for the GCE of 0.07  $\text{cm}^2$ . Then, the gold structures were surface modified with cysteine for the electrostatic immobilization of superoxide dismutase. Using the Laviron analysis [45] based on peak current versus scan rate data from CV, a heterogeneous electron transfer coefficient of  $10 \pm 0.1$   $\text{sec}^{-1}$  was obtained, as well as a transfer coefficient of  $\alpha = 0.5$ . Direct electron transfer was seen between the enzyme and gold surface. Both the reduction and oxidation peak currents for the immobilized enzyme increased upon the addition of superoxide. For a potential of 300 mV (versus Ag/AgCl), a linear range from 0.05 to 440  $\mu\text{M}$  was found, and at  $-200$  mV, a linear range from 0.01 to 540  $\mu\text{M}$  was found, along with a detection limit of 2.1 nM. Figure 7 shows SEM (JSM 7600, JEOL Ltd., Tokyo, Japan) images of these dendritic structures at different deposition times, along with an EDS (energy dispersive spectroscopy) spectrum confirming their gold composition.

Gold nanostructures were formed on the surface of a gold disc electrode by electrodeposition at  $-1.0$  V (versus SCE) from 2.8 mM of  $\text{HAuCl}_4$  in 0.1 M of  $\text{HClO}_4$  for 600 s to form a support for an amperometric  $\text{H}_2\text{O}_2$  sensor using immobilized hemoglobin [77]. At the  $-1.0$  V potential, hydrogen bubbles that formed on the surface served as a dynamic template, resulting in a surface covered by networks of fine dendritic structures with macroporous openings. The roughness factor as determined by the oxide stripping method in 0.5 M of  $\text{H}_2\text{SO}_4$  was 47.7. The gold surfaces were then modified by a SAM of 3-mercaptopropylphosphonic acid and hemoglobin immobilized by adsorption. The immobilized hemoglobin showed direct electron transfer and could be used as an amperometric sensor for  $\text{H}_2\text{O}_2$  operating at  $-0.3$  V with a detection limit of 25 nM and a linear range of 78 nM to 91  $\mu\text{M}$ .

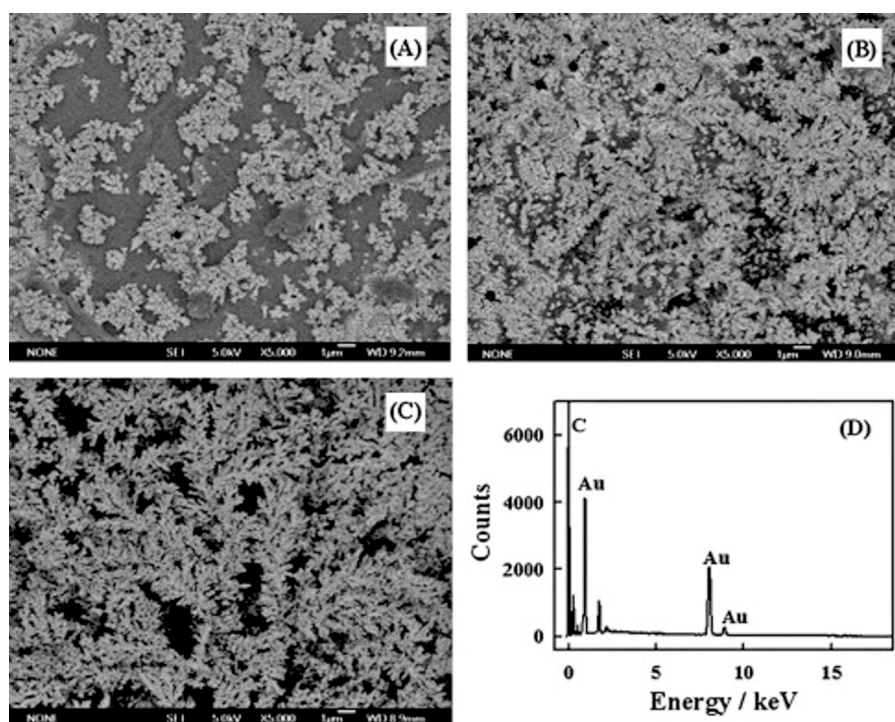


**Figure 7.** Scanning electron microscopy images of the DenAu/GC (dendritic gold/glassy carbon) electrodes with different electrodeposition times of 300 s (A), 500 s (B), and 700 s (C), and the energy dispersive spectroscopy (EDS) spectrum (D) of the DenAu/GC electrode of 700 s. Reproduced with permission from ref. [76], Copyright 2014, Elsevier.

Dendritic gold micro/nanostructures were formed by electrodeposition onto GCE and used as a non-enzymatic sensor for glucose [78]. The deposition time, deposition potential, and  $\text{HAuCl}_4$  concentration were varied, and the effect of these on the deposit morphology examined. At 3600 s and 10 mM of  $\text{HAuCl}_4$ , deposition at 0.3 V (versus Ag/AgCl) produced uniform dispersed flower-like and tetrahedral shapes made of nanoparticles that were three  $\mu\text{m}$  in size. The morphology changed to denser flower-like structures at 0.1 V, to smaller dendritic clusters at  $-0.1$  V, and to denser and longer dendrites at  $-0.3$  V that were microns in length and had feathery branches. Deposition time under these conditions was also examined, and denser dendrites were observed at 5400 s and 7200 s. The morphologies were deemed consistent with growth by diffusion limited aggregation. The conditions of electrodeposition from 10 mM of  $\text{HAuCl}_4$ , at  $-0.3$  V, and for 3600 s were deemed ideal for the electrocatalytic oxidation of glucose. An applied potential of 0.15 V was optimal for detection, balancing sensitivity and stability, and a detection limit of 0.05 mM and a linear range from 0.1 to 25 mM were found.

Dendritic structures of CuNi were formed by electrodeposition onto copper foil and shown to be useful as a potential non-enzymatic glucose sensor [79]. Electrodeposition was carried out from solutions of 0.03 M of  $\text{NiSO}_4$ , 0.03 M of  $\text{CuCl}_2$ , and 0.1 M of  $\text{Na}_2\text{SO}_4$  at a series of potentials from  $-0.6$  V to  $-1.2$  V (versus SCE) for 3600 s. Dendritic structures were obtained. Energy dispersive spectroscopy (EDS) revealed that the Cu/Ni ration varied along the stem of the dendrites, increasing in the direction of dendrite stem growth. Cyclic voltammetry in 0.1 M of NaOH and one mM of glucose confirmed the electrocatalytic oxidation of glucose.

Dendritic gold nanostructures formed on GCE were used as a support for an aptamer-based sandwich assay for thrombin [80]. Dendritic gold nanostructures were electrodeposited onto GCE at  $-0.6$  V (versus SCE) from 0.1 M of  $\text{Na}_2\text{SO}_4$  and 30 nM of  $\text{HAuCl}_4$ . Then, the surfaces were modified by a thiolated anti-thrombin aptamer and 6-mercapto-1-hexanol. Also, 150-nm mesoporous silica nanoparticles (MSN) were prepared, onto which eight-nm Au nanoparticles were formed, and these

particles were loaded with thionine and also modified by the adsorption of an anti-thrombin aptamer. The binding of thrombin to the electrode surface was followed by binding of the aptamer-modified MSN, which allowed for thrombin detection using the detection of thionine using DPV. A detection limit of  $0.5 \text{ ng mL}^{-1}$  for thrombin was achieved, as well as a log-linear range from  $0.03 \text{ pM}$  to  $0.018 \text{ }\mu\text{M}$  thrombin.

Dendritic gold micro/nanostructures grown on ITO-coated glass electrodes were demonstrated as useful for DNA detection [81]. Gold structures were electrodeposited from  $12 \text{ mM}$  of  $\text{HAuCl}_4$  and  $0.05 \text{ M}$  of  $\text{HClO}_4$  at potentials ranging from  $0.3 \text{ V}$  to  $-0.3 \text{ V}$  (versus  $\text{Ag}/\text{AgCl}$ ) and times from two to  $15 \text{ min}$ . A comparison of structures deposited at a constant amount of charge passed of  $0.2 \text{ C}$  showed a trend toward a more dendritic morphology as the deposition potential became more negative up until  $-0.1 \text{ V}$ ; then, at  $-0.3 \text{ V}$ , the structures appeared more irregular and less branched. The gold surfaces were modified by a thiolated 18-mer complementary DNA strand followed by treatment with 6-mercapto-1-hexanol. The binding of a target DNA, and subsequently a reported DNA bound to gold nanoparticles, were monitored by using the electrochemical response of a bound methylene blue redox indicator by square-wave voltammetry. The response has a log-linear range from  $50 \text{ aM}$  to one  $\text{pM}$ , and a detection limit of  $12 \text{ aM}$ .

Dendritic silver structures formed on gold foil by electrodeposition were shown to have electrocatalytic activity for the reduction of  $\text{H}_2\text{O}_2$  [82]. The dendritic structures were formed by electrodeposition at  $-0.3 \text{ V}$  (versus  $\text{Ag}/\text{AgCl}$ ) at times of  $10 \text{ s}$ ,  $60 \text{ s}$ , or  $120 \text{ s}$ . XRD confirmed that the Ag dendrites were of crystalline silver. The dendrites were about eight  $\mu\text{m}$  long, with branches that were  $70$  to  $80 \text{ nm}$  in diameter.

The electrodeposition of Au nanostructures in the presence of cysteine onto ITO-coated glass was found to trend toward more bumpy and dendritic structures at longer deposition times [83]. The number of particles deposited in  $60 \text{ s}$  increased as the potential became more negative, from  $16 \mu\text{m}^{-2}$  at zero  $\text{V}$  (versus  $\text{Ag}/\text{AgCl}$ ), to  $160 \mu\text{m}^{-2}$  at  $-0.3 \text{ V}$ , and to  $400 \mu\text{m}^{-2}$  at  $-0.5 \text{ V}$ . Deposition was carried out from  $0.5 \text{ M}$  of  $\text{H}_2\text{SO}_4$  with  $2 \text{ mM}$  of  $\text{NaAuCl}_4$  and  $0.125 \text{ mM}$  of L-cysteine as a structure-directing agent. The size decreased with more negative potential from  $83 \pm 38 \text{ nm}$  at zero  $\text{V}$ , to  $39 \pm 13 \text{ nm}$  at  $-0.3 \text{ V}$ , and to  $22 \pm 9 \text{ nm}$  at  $-0.5 \text{ V}$ . The gold nuclei clearly form more rapidly at lower applied potential, as expected. Deposition at zero  $\text{V}$  and at longer times up to  $1800 \text{ s}$  resulted in a trend in morphology to bumpy, and then ultimately dendritic structures. The bumpy structures formed at  $60 \text{ s}$  had a plasmon absorbance peak refractive index sensitivity of  $163 \text{ nm}$  of  $\text{RIU}^{-1}$ .

#### 4.2. Nanostructures Described as 'Flower-Like', Irregular, of Unusual Morphology

A nanostructure formed on gold electrodes by first electrodepositing gold nanocorrals followed by electrodepositing platinum nanoflowers provided an amperometric  $\text{H}_2\text{O}_2$  sensor of good sensitivity operating at a low potential [84]. Gold nanocorrals that were formed by electrodeposition at  $-3.0 \text{ V}$  (versus  $\text{Ag}/\text{AgCl}$ ) in solution of  $0.01 \text{ M}$  of  $\text{HAuCl}_4$  and  $2.5 \text{ M}$  of  $\text{NH}_4\text{Cl}$  for  $120 \text{ s}$  were created by using the hydrogen bubbles formed at this highly negative potential as a template [85]. The resulting nanocorrals were examined by SEM (Merlin, Carl Zeiss AG, Oberkochen, Germany) and showed a honeycomb-like structure of large pores of  $\sim 50 \mu\text{m}$  whose walls were an agglomeration of small gold nanoparticles that formed in the interstitial spaces between the hydrogen bubbles, which then detach and leave behind a porous structure. In order to achieve these structures, it was noted that a low concentration of  $\text{HAuCl}_4$  was required, because otherwise, dendrites would form. The platinum nanoflowers were formed on the gold nanocorrals by electrodeposition in  $25 \text{ mM}$  of  $\text{H}_2\text{PtCl}_6$  and  $50 \text{ mM}$  of  $\text{H}_2\text{SO}_4$  at  $-1 \text{ V}$  for  $90 \text{ s}$ , while platinum nanospheres would form on the gold nanocorrals if electrodeposition took place in a solution of  $25 \text{ mM}$  of  $\text{K}_2\text{PtCl}_4$  and  $50 \text{ mM}$  of  $\text{H}_2\text{SO}_4$  at  $-0.2 \text{ V}$  for  $200 \text{ s}$ . The gold nanocorrals decorated with platinum nanoflowers had the superior sensitivity for the oxidation of  $\text{H}_2\text{O}_2$  at a potential of  $0.15 \text{ V}$ . Glucose oxidase was immobilized by cross-linking with glutaraldehyde to make a first-generation glucose biosensor with a linear range of  $0.01$  to  $2.0 \text{ mM}$  and

good sensitivity. Figure 8 shows SEM images of gold nanocorrals alone and decorated with platinum nanoflowers and platinum nanospheres.

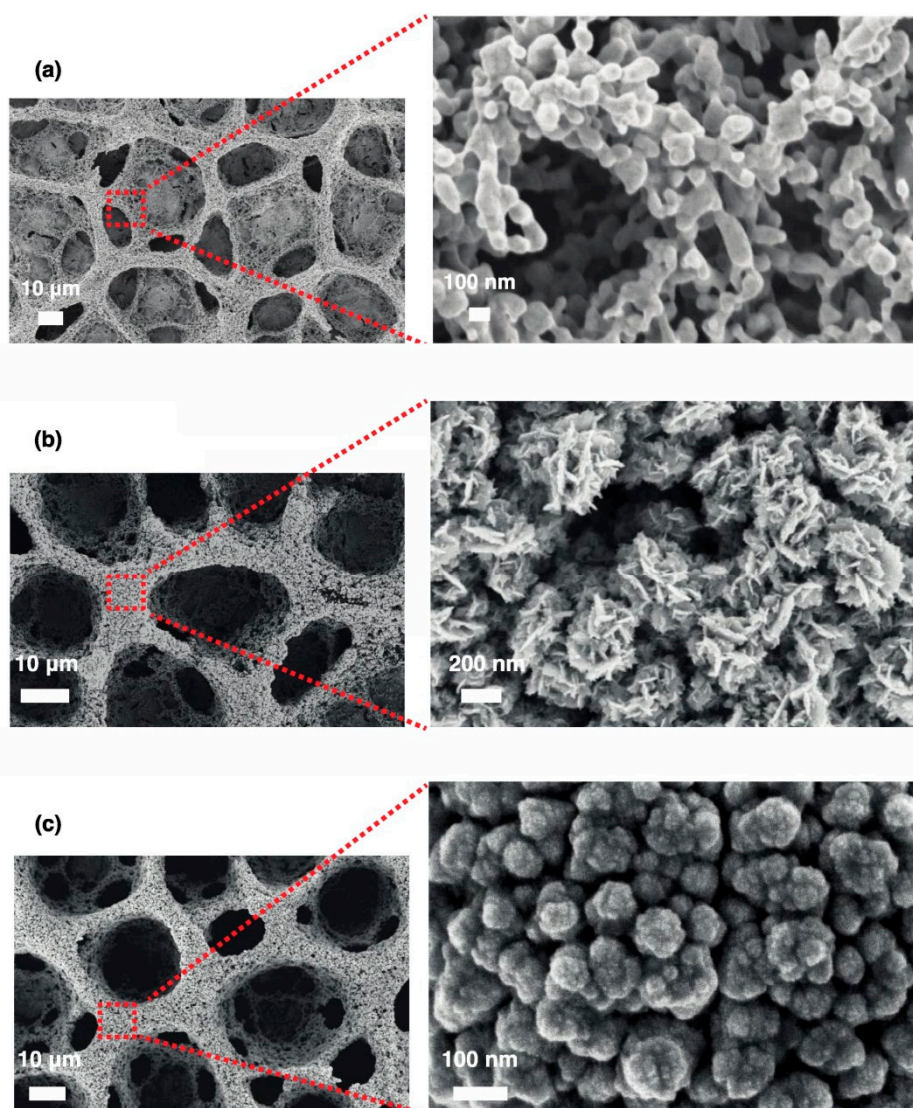


**Figure 8.** SEM images of (a) Au nanocorrals, (b) Au nanocorrals with Pt nanoflowers (−1 V for 90 s from tetravalent Pt), and (c) with Pt nanospheres (−0.2 V for 200 s from divalent Pt). Reproduced with permission from ref. [84], Copyright 2017, Elsevier.

Cauliflower-shaped gold nanoparticles were formed on SPCE and used to make an electrochemical immunosensor [86]. A solution of 0.25 mM of Au(III) was used, and the potential that was applied to the SPCE was swept from 0.8 V to 0 V (versus Ag/AgCl) over up to 15 cycles. The well-separated cauliflower-shaped nanoparticles grew on edges on the carbon surface and increased in size with the number of cycles, and were shown in the range of 15 to 61 nm. Then, a ferrocene-conjugated lipoic acid derivative was immobilized onto the gold surfaces. Then, antibodies against human IgG were immobilized and covered by bovine serum albumin. The binding of antigen resulted in an increase in peak current from the oxidation of the ferrocene units, which was attributed to a conformational change upon binding. The immobilization of HRP for the detection of H<sub>2</sub>O<sub>2</sub> oxidation was also reported.

Electrodeposition under different conditions onto boron-doped diamond electrodes was used to produce three distinct morphologies that resulted in different electrochemical behavior for immobilized hemoglobin [87]. Electrodeposition from two mM of HAuCl<sub>4</sub> at 0.5 V (versus Ag/AgCl) resulted in

flower-like deposits 100 to 150 nm in size and with XRD patterns that had a dominant Au(111) peak in addition to Au(200) and Au(220) peaks. In contrast, electrodeposition at the same potential from 0.2 mM of H<sub>2</sub>AuCl<sub>4</sub> gave spherical nanoparticles that were 70 to 100 nm in size for which the Au(111) XRD peak was smaller than in the flower-like structures. Changing the deposition potential to −0.1 V with 2 mM of H<sub>2</sub>AuCl<sub>4</sub> resulted in convex nanoparticles with a grain size of 150 to 200 nm, and yet less intense Au(111) XRD peaks. Cyclic voltammetry of the three nanostructures showed differing contributions of oxidation peaks at +1.1 V due to Au(200) or Au(220) crystal facets and at +1.4 V due to Au(111) facets. For immobilized hemoglobin, which was analyzed using the Laviron analysis of the cyclic voltammetry data, resulted in different electron transfer rates of 0.34 sec<sup>−1</sup>, 0.16 sec<sup>−1</sup>, and 0.13 sec<sup>−1</sup> on flower-like, spherical, and convex nanoparticles, respectively.

Platinum nanopetal structures were formed by electrodeposition onto either Pt screen-printed electrodes or platinum electrodes, and used to make a glucose sensor based on the detection of H<sub>2</sub>O<sub>2</sub> produced by the enzyme glucose oxidase [88]. Electrodeposition parameters regarding concentration, potential, and time were systematically varied for electrodeposition from solutions of H<sub>2</sub>PtCl<sub>6</sub> in H<sub>2</sub>SO<sub>4</sub> or for K<sub>2</sub>PtCl<sub>4</sub> in H<sub>2</sub>SO<sub>4</sub>. Electrodeposition at −1.0 V (versus Ag pseudoreference) from 25 mM of H<sub>2</sub>PtCl<sub>6</sub> and 50 mM of H<sub>2</sub>SO<sub>4</sub> gave nanopetals with a size of 68 ± 20 nm. Electrodeposition from 25 mM of K<sub>2</sub>PtCl<sub>4</sub> and 50 mM of H<sub>2</sub>SO<sub>4</sub> at −0.2 V resulted in regular nanospheres with a size of 52 ± 18 nm. Lowering the potential to −2.0 V resulted in the formation of nanopetals from the K<sub>2</sub>PtCl<sub>4</sub> solution. Hybrid structures made by electrodepositing nanopetals over the nanospheres were found to be the most sensitive for the non-enzymatic amperometric detection of glucose. Glucose oxidase immobilized by casting from a solution containing glutaraldehyde resulted in a first-generation (H<sub>2</sub>O<sub>2</sub> detection) glucose sensor operating at +0.7 V (versus Ag/AgCl). The Pt nanopetals were covered by a K<sup>+</sup> sensitive polyvinyl chloride membrane, and used as an ion-selective electrode to detect K<sup>+</sup> released by cells undergoing osmotic shock [89].

Flower-shaped gold nanostructures were formed by electrodeposition onto silanized ITO-coated glass electrodes, and found to be sensitive substrates for the detection of dopamine by surface-enhanced Raman spectroscopy [90]. The ITO-coated glass was first silanized with a monolayer of aminopropyltrimethoxysilane followed by electrodeposition using a two-second nucleation step at 0.7 V (versus SCE) followed by 600 s at −0.4 V from 0.5 to 1.0 mM of H<sub>2</sub>AuCl<sub>4</sub>. The result was gold ‘nanoflower’ shapes with a size of 300 to 600 nm.

Hierarchical gold nanostructures were formed by electrodeposition in which the pH of the solution and the temperature were used to control the morphology [91]. From 5 mM of H<sub>2</sub>AuCl<sub>4</sub>, deposition at 0.5 V (versus SCE) onto GCE for 10 min at pH 2–3 gave popcorn-like morphologies that were aggregates of nanocrystals. At pH 4, deposition produced waxberry nanostructures that were 600 nm in size and made of 30 nm nanocrystals. Deposition at 40 °C gave waxberry nanostructures of 1 μm size with some nanoparticles linking in between. At pH 6, irregular structures were formed. The change in pH favored different Au complexes in solution with different redox potentials and growth rates, with AuCl<sub>4</sub><sup>−</sup> dominant at lower pH and Au(OH)<sub>4</sub><sup>−</sup> at higher pH. The structures formed at pH 4 and 40 °C were very active for the electrocatalytic oxidation of glucose, with detection at 0.36 V giving a linear range from two to 38 mM and a detection limit of 4 μM.

Anisotropic Au nanoparticles were formed by electrodeposition and used as a support for a DNA sensor for *Trichomonas Vaginalis* [92]. The nanoparticles were formed by electrodeposition from 0.5 M of H<sub>2</sub>SO<sub>4</sub> with 20 mM of H<sub>2</sub>AuCl<sub>4</sub> and 150 mM of phenobarbital at 0.0 V (versus Ag/AgCl) for 300 s. The modification of the surface with the anisotropic Au nanoparticles resulted in a roughness factor of 6.0. The gold surfaces were modified with a thiolated probe oligonucleotide and mercaptohexanol. The toluidine blue redox probe that binds preferentially to dsDNA was used together with DPV, and a detection limit of 3.1 × 10<sup>−20</sup> M and a log-linear range of 1.0 × 10<sup>−19</sup> M – 1.0 × 10<sup>−12</sup> M for the complementary strand were achieved. The anisotropic Au nanoparticles were also used as support for a DNA sensor for *Leishmania infantum* [93]. In contrast, the use of the polyamine spermidine as a structure-directing agent resulted in the formation of gold nanoleaves on a gold electrode surface

for modification by a thiolated DNA probe for detection of *Leishmania major* using differential pulse voltammetry and the methylene blue redox probe [94]. A detection limit of  $1.8 \times 10^{-20}$  M was found for a synthetic complimentary strand, and a detection limit of  $0.07 \text{ ng mL}^{-1}$  was found for the genomic DNA from the protozoa.

Using cadaverine (1,5-pentanediamine) as a structure-directing agent, hairbrush-like gold nanostructures were formed by electrodeposition and used as a platform for an aptamer-based sensor for a prostate-specific antigen [95]. The deposition onto a gold electrode was carried out from 500 mM of  $\text{H}_2\text{SO}_4$ , 150 mM of cadaverine, and 20 mM of  $\text{HAuCl}_4$  at zero V (versus Ag/AgCl) for 600 s. The surface that was produced consisted of hairbrush-like rods that were made of 30 to 150-nm spindles. The thiolated aptamer against prostate specific antigen (PSA) was immobilized along with 6-mercapto-1-hexanol. The binding of PSA to the aptamer resulted in a change in its folding, bringing the redox probe methylene blue closer to the electrode surface and resulting in an increase in peak current in DPV. A linear range for PSA detection from  $0.125$  to  $125 \text{ ng mL}^{-1}$ , and a detection limit of  $0.04 \text{ ng mL}^{-1}$  was achieved.

Fractal tree-like nanostructures formed by electrodeposition onto ITO-coated glass were first modified by a polyelectrolyte layer that was formed by alternating the deposition of anionic polystyrene sulfonate and poly(diallyldimethylammonium chloride), and then used as the support for a sensor for human apolipoprotein E4, which is of diagnostic value for Alzheimer's disease [96]. The electrodeposition was done for 1800 s from  $10 \text{ mg mL}^{-1}$  of  $\text{HAuCl}_4$  in 0.5 M of  $\text{H}_2\text{SO}_4$  at  $-1800 \text{ mV}$  (versus Ag/AgCl). The fractal shapes were five to  $10 \text{ }\mu\text{m}$  in length, had an overall height of 15 to  $26 \text{ }\mu\text{m}$ , and were composed of many  $\sim 10\text{-nm}$  nanoparticles. Antibodies against the APOE-4 isoform were immobilized on the gold surfaces by adsorption. The APOE-4 protein would bind between the surface-immobilized antibodies and antibodies conjugated to HRP. Detection, using the addition of  $\text{H}_2\text{O}_2$  and hydroquinone as a mediator, gave a detection limit of  $0.3 \text{ ng mL}^{-1}$ .

Fractal-shaped gold nanostructures with high ramification were found to be more efficient at capturing cancer cells than less ramified structures [97]. The structures were deposited onto ITO-coated glass that was precoated with a layer of poly(acrylic acid) and poly(ethylenimine) at either  $-0.1 \text{ V}$ ,  $-0.15 \text{ V}$ , or  $-0.3 \text{ V}$  (versus Ag/AgCl) for 180 min or 30 min from  $1 \text{ mg mL}^{-1}$  of  $\text{HAuCl}_4$ . The most ramified structures were produced at  $-0.3 \text{ V}$  and 30 min. The structures were about  $5 \text{ }\mu\text{m}$  in size, and were characterized by a fractal dimension by image analysis. The surfaces were modified with a thiol-PEG-biotin derivative to which streptavidin would bind, and then, a biotinylated antibody against EpCam as well. EpCam is overexpressed on the surface of cancer cells, and the most ramified gold structures had the highest efficiency regarding the capture of MCF7 breast cancer cells.

The electrodeposition of gold nanopikes onto Au-coated Si wafers resulted in substrates with great anti-bacterial efficiency [98]. Electrodeposition from 6.8-mM  $\text{HAuCl}_4$  and one mM of  $\text{Pb}(\text{CH}_3\text{COO})_2$  resulted in the formation of nanopikes, which were characterized by their spacing, height, cap radius, base radius, surface density, and roughness. Increasing deposition time at  $0.05 \text{ V}$  (versus Ag/AgCl) over 260 s, 540 s, 720 s, and 900 s resulted in increases in all of the geometric parameters, but a decrease in the surface density. At the longest deposition time, the nanopikes were  $555 \pm 214 \text{ nm}$  in height and had a  $103 \pm 82$  cap radius. For the nanopikes deposited at a time of 540 s, a near 90% efficiency for killing *P. Aeurunginosa* bacteria was observed.

#### 4.3. Electrodeposition of Single Ramified Nanostructures Through Apertures

Electrodeposition through microscale apertures enables the possibility of creating arrays of individually addressable nanostructures. The study of individual nanostructures allows insight into the relation between their size and morphology and their analytical response. The electrodeposition of nanostructured gold microdeposits onto a gold surface through  $10\text{-}\mu\text{m}$  apertures produced using photolithography was studied as a function of gold ion concentration, solution viscosity, and deposition potential in order to determine the conditions that would lead to an optimal response for the electrochemical detection of DNA hybridization (duplex formation) [99]. It was reasoned that the

larger areas of structures that protruded out into solution would increase the frequency of biomolecular encounters and also make the transport of redox probes more efficient by radial diffusion. The quantity of gold that was deposited was kept constant across all of the structures by adjusting the deposition time. The concentration of  $\text{HAuCl}_4$  was varied from one to 500 mM in 0.5 M of HCl. Using 50 mM of  $\text{HAuCl}_4$ , the potential was varied from 500 mV to  $-700$  mV. Viscosity was varied by preparing the solution to be up to 75% glycerol, with electrodeposition carried out at zero V and in 50 mM of  $\text{HAuCl}_4$ . Depending on the conditions, the electrodeposited structures were classified as roughened hemispheres, twinned leaves, pentagonal needles, or amorphous growth. As the concentration of  $\text{HAuCl}_4$  increased, the morphology of the electrodeposited structures evolved from rounded but with distinct lobes to leaf-like and covered with geometric patterns, and then to needles that became smoother at high concentrations. An increase in the viscosity of the solution resulted in more compact structures. Variation of the electrodeposition potential resulted in an evolution in morphology from hemispherical to needle-like to spiky to flaky. Then, the structures were surface modified with a thiolated DNA strand, and hybridization was monitored using methylene blue as a redox probe. The rate of DNA hybridization was fastest on the finer, spiky nanostructures.

Nanostructured microelectrode arrays of Pd were fabricated by electrodeposition and used as DNA sensors [100,101]. The single nanostructures were grown onto gold surfaces exposed through 500-nm apertures produced using photolithography on a  $\text{SiO}_2$  layer on a gold-coated silicon chip. The parameters of  $\text{H}_2\text{PdCl}_4$  concentration, electrolyte solution, deposition potential, and time were varied to produce structures of about 10  $\mu\text{m}$  in size, which were classified either as smooth, moderately rough (nanostructured on a 100 to 300-nm length scale), or finely rough (nanostructured on a 20 to 50-nm length scale). The structures were surface modified by a thiolated peptide nucleic acid that was chosen for its neutral charge, which enhanced the response of the reporter system redox probes. The binding of a complimentary 20-mer DNA strand was monitored using an electrocatalytic reporter system consisting of 10  $\mu\text{M}$  of  $[\text{Ru}(\text{NH}_3)_6]^{3+}$  and four  $\mu\text{M}$  of  $[\text{Fe}(\text{CN})_6]^{3-}$ . The electrode array had eight individually addressable nanostructures exhibiting ideal microelectrode behaviors. The finely rough nanostructures had the lowest detection limit of 10 aM for the complimentary DNA strand with a log-linear range from one to 100 aM. The hybridization kinetics were fastest on the finely rough nanostructures. A change in the Pd particle structure from smooth to nanostructured reduced the detection limit for 20-mer DNA from 100 fM to one fM [102]. The Pd nanostructured microelectrode arrays were also modified with peptide nucleic acids and applied to the detection of gene fusion sequences that are unique to prostate cancer and were taken from prostate cancer tissue [103]. A study comparing the hybridization efficiency and ssDNA surface coverage on the extent of the nanostructuring of the Pd surface found that the most nanostructured surface had the highest hybridization efficiency, and that the hybridization efficiency on a spherical surface was very low [104]. Figure 9 shows SEM images of the individual palladium nanostructures, which were classified as smooth, moderately nanostructured, and highly nanostructured.

Nanostructured microelectrode arrays of gold were fabricated in a similar manner and used to detect mRNA in the form of a gene fusion from chronic myeloid leukemia [105]. The apertures through which the electrodeposition was done were five  $\mu\text{m}$  in size, and 100- $\mu\text{m}$  spiky and dendritic structures were formed. Electrodeposition was conducted at 0 V for 175 s from 20 mM of  $\text{HAuCl}_4$  in 0.5 M of HCl. The surfaces were modified by a thiolated peptide nucleic acid probe and 6-mercapto-1-hexanol. Using the catalytic reporter system of 10  $\mu\text{M}$  of  $[\text{Ru}(\text{NH}_3)_6]^{3+}$  and four  $\mu\text{M}$  of  $[\text{Fe}(\text{CN})_6]^{3-}$ , it was possible to detect the mRNA from as few as 10 lysed cancer cells using DPV.

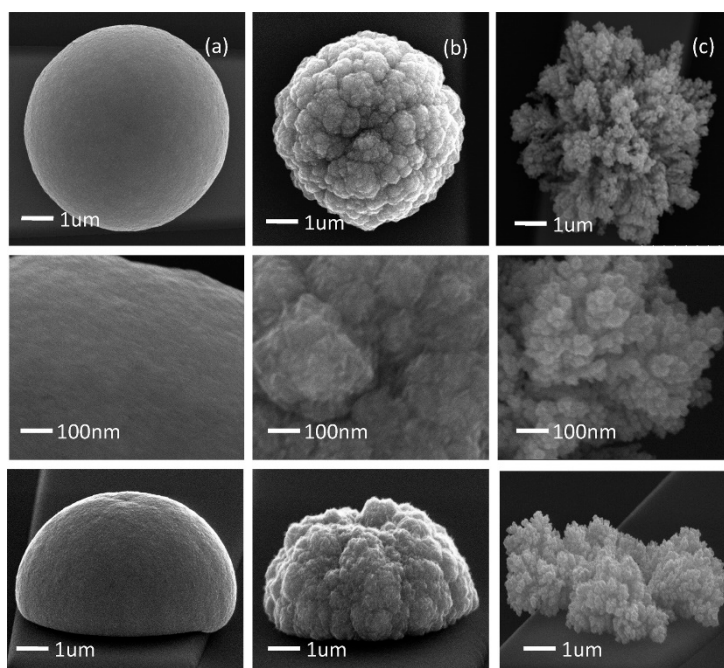


**Figure 9.** The scanning electron microscopy (SEM) images of three Pd NMEs (nanostructured microelectrodes) fabricated with different levels of nanostructuring: (a) smooth surfaces, (b) moderately nanostructured surface with a feature size of 100 to 150 nanometers, and (c) finely nanostructured surface with a feature size of 20 to 30 nanometers. Reproduced with permission from ref. [104], Copyright 2010, American Chemical Society.

Nanostructured microelectrode arrays were used to make biosensors for the protein antigen CA-125, which is a biomarker for ovarian cancer [106]. Gold nanostructures of different sizes (eight  $\mu\text{m}$ , 30  $\mu\text{m}$ , and 100  $\mu\text{m}$ ) were prepared on microchips through five- $\mu\text{m}$  apertures by electrodeposition. The 100- $\mu\text{m}$  structures were formed by electrodeposition at zero V for 200 s from 20 mM of  $\text{HAuCl}_4$  in 0.5 M of HCl, the 30- $\mu\text{m}$  structures were formed by electrodeposition from this solution at 150 mV for 200 s, and the eight- $\mu\text{m}$  structures were formed by chronoamperometry at 30 nA for 50 s. The eight- $\mu\text{m}$  structures had a fuzzy shape, the 30- $\mu\text{m}$  structures were spikey in appearance, and the 100- $\mu\text{m}$  ones were of a more dendritic nature. The gold surfaces were modified by cystamine, followed by activation with glutaraldehyde for immobilization of the anti-CA 125 antibody. The blocking of the redox current from a solution of 2.5 mM of  $\text{K}_3[\text{Fe}(\text{CN})_6]$  and 2.5 mM of  $\text{K}_4[\text{Fe}(\text{CN})_6]$  upon binding of CA-125 to the antibody was used for detection. The eight- $\mu\text{m}$  size structures enabled the detection of as low as 0.1 U  $\text{mL}^{-1}$  of CA-125 where 0.1 U = 500 fM, while the 30- $\mu\text{m}$  structures allowed the detection of one U  $\text{mL}$ , and the 100- $\mu\text{m}$  structures allowed the detection of 10 U  $\text{mL}^{-1}$ .

Si chips that were patterned with Au working, reference, and auxiliary electrodes were modified with gold nanostructures, also through five- $\mu\text{m}$  apertures, and used to detect DNA from bacteria [107]. The nanostructures were electrodeposited at -700 mV for 10 s from 20 mM of  $\text{HAuCl}_4$  in 0.5 M of HCl. Then, the nanostructures were modified by peptide nucleic acid. The device contained a special lysis chamber, allowing for the lysis of bacteria, followed by detection down to a level of one CFU per  $\mu\text{L}$ . The total time for analysis, from lysis to detection of the bacterial DNA, was less than 30 min [108]. The use of gold instead of palladium was needed to produce structures extending 100  $\mu\text{m}$  into the solution.

## 5. Biosensor Application of Electrodeposited Composite Nanostructures

There are many reasons for preparing films on electrode surfaces for biosensor application that contain multiple structural and functional components. For example, the preparation of composite nanostructured films containing both metallic nanoparticles and carbon nanomaterials such as



graphene or carbon nanotubes allows for enhanced conductivity within the structure. Graphene, with its superior conductivity and electron transfer capacity, is a recent and popular choice, as are carbon nanotubes. Prussian blue, when deposited along with metallic nanoparticles, improves electrocatalytic properties. Conducting polymers can also aid the conductivity and electronic properties of electrode coatings. Other polymers including Nafion or chitosan may improve the film-forming ability and stability of protected components.

### 5.1. Composite Electrodes Containing Carbon Nanomaterials

A composite nanostructured layer containing copper nanoparticles, multiwalled carbon nanotubes (MWCNT), and chitosan was formed on gold wire electrodes as a support for a biosensor based on sarcosine oxidase [109]. Carboxylated MWCNT (c-MWCNT) dispersed in 3:1 H<sub>2</sub>SO<sub>4</sub>:HNO<sub>3</sub> were mixed with an aqueous solution of EDC and NHS of pH 6.0. Chitosan was electropolymerized onto the gold electrode by applying 20 cycles from  $-1.1$  to  $0.1$  V (versus Ag/AgCl). A suspension of copper nanoparticles (average size: 50 nm) and c-MWCNT was then electrodeposited by applying 20 cycles of  $-1.1$  to  $0.1$  V at  $20$  mV sec<sup>-1</sup>. Sarcosine oxidase was immobilized onto the activated composite electrodes and used as an amperometric sensor for sarcosine, which was noted as present in urine and blood during prostate cancer, with a detection limit of  $0.1$  pM.

A biosensor for the detection of DNA hybridization based on electrochemiluminescence was constructed from a complex composite structure [110]. Carbon nanotubes were first deposited onto a GCE. Au/Pt nanoparticles were electrodeposited at  $-0.2$  V for 200 s in a solution of  $1.0$  mM of H<sub>2</sub>AuCl<sub>4</sub> and  $1.0$  mM of H<sub>2</sub>PtCl<sub>6</sub>. Then, a capture DNA probe was assembled onto the surface, including the use of mercaptohexanol to promote improved probe orientation. After hybridization with the target DNA, a DNA-modified nanosheet of graphite-like carbon nitride nanosheets (g-C<sub>3</sub>N<sub>4</sub>) modified with gold nanoparticles was bound to the duplex. The assembly generated an electrochemiluminescence signal that was detected while scanning the potential from  $0$  to  $-1.5$  V for 10 cycles at  $100$  mV sec<sup>-1</sup>. A linear range from  $0.04$  to  $5.0 \times 10^4$  fM and a detection limit of  $0.018$  fM were observed. The detection of DNA spiked into serum samples was also reported.

A complex nanocomposite electrode was formed by one-step electrodeposition in order to prepare a highly sensitive first-generation glucose sensor [111]. As a first step, graphene oxide was dispersed, and H<sub>2</sub>PtCl<sub>4</sub> was added, followed by formic acid; then, after 12 days, a dispersion of reduced graphene oxide (rGO) and platinum nanoparticles was obtained at pH 4, and then drop cast onto the gold electrode. Subsequently, electrodeposition was carried out from a solution of  $5.0$  mg mL<sup>-1</sup> of glucose oxidase,  $84$  mM of the ionic liquid imidazolium alkoxysilane,  $0.5\%$  chitosan, and  $30$  mM of benzoquinone by conducting cyclic voltammetry scans between  $0.7$  V and  $-0.8$  V (versus SCE). The electrodes were characterized by SEM (S4800, Hitachi, Tokyo, Japan), FTIR (Nexus 670, Nicolet, Madison, WI, USA) and Raman spectroscopy (Invia, Renishaw, Wotton-under-Edge, UK). SEM showed rGO sheets with dispersed platinum nanoparticles. The amperometric response to H<sub>2</sub>O<sub>2</sub> was evaluated and found to be maximal at  $0.55$  V and for films formed on the gold electrode by 10 potential cycles. The sensor was found to have a very low detection limit for glucose of  $0.02$  μM and a linear range from  $0.002$  to  $5.5$  mM.

An impedimetric sensor for tumor necrosis factor alpha (TNF-α) was constructed based on the electrodeposition of reduced graphene oxide and then gold nanoparticles onto ITO electrodes [112]. The rGO was electrodeposited from a  $1$  mg mL<sup>-1</sup> dispersion by cyclic voltammetry conducted between zero and  $-1.6$  V (versus Ag/AgCl) at  $25$  mV sec<sup>-1</sup>. Subsequently, gold nanoparticles were electrodeposited from  $0.5$  mM of H<sub>2</sub>AuCl<sub>4</sub> at  $-0.9$  V for 30 s. Examination by atomic force microscopy (PSIA XE-100, Park Systems, Seoul, South Korea) showed that the rGO only covered surfaces that showed sheet-like structures of  $37$ -nm thickness, the electrodeposition of only gold nanoparticles showed particles about  $170$  nm in size, and the composite of rGO and gold nanoparticles showed aggregated structures on the surface. Then, the surface was modified with 3-mercaptopropionic acid, and an anti-TNF-α antibody was covalently linked by amide bonds that were formed using EDC/NHS

chemistry. The binding of TNF- $\alpha$  was followed using Faradaic impedance spectroscopy with the  $\text{Fe}(\text{CN})_6^{3-/4-}$  redox probe and using the change in resistance at one Hz as the response, a detection limit for TNF- $\alpha$  of  $0.43 \text{ pg mL}^{-1}$  was obtained, which was below the  $10$  to  $30 \text{ pg mL}^{-1}$  that is expected in human serum.

An electrochemical sensor for  $\text{H}_2\text{O}_2$  was constructed by electrodepositing bimetallic nanoparticles of gold and platinum onto reduced graphene sheets that had been drop cast onto a GCE surface and then dried under an infrared lamp [113]. The film of nanoparticles was electrodeposited by cyclic voltammetry in a solution of two mM of  $\text{H}_2\text{PtCl}_6$  and one mM of  $\text{HAuCl}_4$  also containing the surfactant Brij 58 at 1.0 wt%. The potential was scanned from 0.4 V to  $-0.5 \text{ V}$  at  $100 \text{ mV sec}^{-1}$  for five cycles. If electrodeposition was carried out only from  $\text{HAuCl}_4$  in solution, aggregated nanoparticles formed, and if carried out from  $\text{H}_2\text{PtCl}_6$  solution, only very few particles formed. However, when carried out from the mixed solution, more uniformly dispersed nanoparticles were seen in SEM (Sirion 200, FEI Inc., Eindhoven, Netherlands). The current response to  $\text{H}_2\text{O}_2$  was maximal when the ratio of Au/Pt was 1:2, and for this, composition was maximal for five cycles conducted at  $100 \text{ mV sec}^{-1}$ . Under these conditions, the nanoparticles were dispersed, and the surface area was maximized. Response to  $\text{H}_2\text{O}_2$  at zero V gave a limit of detection of 0.31 mM, and a linear range from one to 1.78 mM, and another linear range of a lower slope from 1.78 to 16.8 mM. The sensor was used to measure  $\text{H}_2\text{O}_2$  released from rat pheochromocytoma cells (PC 12) cancer cells.

The electrodeposition of gold nanoparticles onto a GCE covered by a drop-cast layer of multiwall carbon nanotubes followed by adsorption of glucose oxidase was used to create a modified electrode useful both as a glucose biosensor and as a bioanode in a glucose fuel cell [114]. The multiwalled carbon nanotubes were modified with  $-\text{NH}_2$  groups and were 13 to 18 nm in diameter and one to 12- $\mu\text{m}$  long. Gold nanoparticles were electrodeposited from  $\text{KAuCl}_4$  solution and were 10 to 25 nm in size, and were seen by SEM (S-4700, Hitachi, Tokyo, Japan) to decorate the nanotubes. Adsorbed glucose oxidase resulted in a highly sensitive glucose biosensor with a detection limit of 0.5 mM and a linear range from one to 24 mM. The modified GCE was used as a bioanode, with the GCE modified by carbon nanotubes and gold nanoparticles giving the best performance as the biocathode.

Acetylcholinesterase and choline oxidase were immobilized in a composite film and used to create a sensor for acetylthiocholine chloride based on electrochemiluminescence [115]. Electrodeposition onto a GCE was carried out from a dispersion of graphene oxide sheets with dissolved  $\text{HAuCl}_4$  and chitosan by conducting 10 cycles between  $-1.6 \text{ V}$  and  $0.6 \text{ V}$  (versus Ag/AgCl) at  $50 \text{ mV sec}^{-1}$ . SEM images showed sheet-like structures with dispersed nanoparticles. A dispersion of  $\text{Fe}_3\text{O}_4$  nanoparticles decorated by smaller  $\text{TiO}_2$  nanoparticles was prepared and then surface modified with aminopropyltrimethoxysilane. Subsequently, the enzymes acetylcholinesterase and choline oxidase were immobilized onto these composite nanoparticles by cross-linking with glutaraldehyde. The dispersion was then drop cast onto the modified electrode to complete the composite film. SEM confirmed the structure of aggregates of larger  $\text{Fe}_3\text{O}_4$  nanoparticles surrounded by  $\text{TiO}_2$  nanoparticles. The combination of these different nanomaterials was designed to enhance the response to  $\text{H}_2\text{O}_2$  that was formed from the reaction sequence in which acetylcholinesterase converts acetylthiocholine to thiocholine, and choline oxidase then converts the thiocholine and  $\text{H}_2\text{O}_2$ , which will partake in the luminol reaction sequence that ultimately yields luminescence. Using acetylthiocholine chloride as the substrate, detection of the ECL signal upon scanning the potential continuously between 0.2 and 0.8 V at  $100 \text{ mV sec}^{-1}$  gave a sensor with a detection limit of  $0.022 \text{ }\mu\text{M}$  and a linear range from 0.0067 to  $921 \text{ }\mu\text{M}$ .

An electrochemical sensor for the organophosphate pesticide Phoxim was developed based on a composite electrode of reduced graphene oxide and Au nanoparticles formed on a GCE [116]. Reduced graphene oxide was first electrodeposited by 500 cycles of pulsed electrodeposition in which the potential was stepped between  $-1.3 \text{ V}$  and  $0.6 \text{ V}$  (versus Ag/AgCl) and held for two seconds, and then stepped back and held for two seconds. Then, the electrodeposition of gold nanoparticles was carried out for 60 s at  $-0.2 \text{ V}$  in a solution of 1%  $\text{HAuCl}_4$  in 0.5 M of  $\text{H}_2\text{SO}_4$ . SEM (SUPRA 55, Carl Zeiss AG,

Oberkochen, Germany) showed flake-like and wrinkled shapes for the rGO sheets covered by Au nanoparticles with an average diameter of 35 nm. Phoxim could be reduced on this modified electrode with a peak current near  $-0.69$  V. Using DPV, a detection limit of  $0.003 \mu\text{M}$  was found for phoxim.

A biosensor for a segment of DNA from hepatitis B virus (HBV) was made based on gold nanoparticles electrodeposited onto a GCE modified with both graphene and carboxylated multiwalled carbon nanotubes (c-MWCNT) [117]. A suspension of graphene oxide and c-MWCNT was first drop cast onto a GCE; then, a potential sweep from zero V to  $-1.5$  V (versus Ag/AgCl) was used to reduce graphene oxide to graphene. Then, gold nanoparticles were formed on the surface by electrodeposition from  $2.9$  mM of  $\text{HAuCl}_4$  at  $-0.2$  V for times varied from 200 to 1000 s. An electrodeposition time of 900 s was found to optimize the surface area. A thiolated hairpin DNA probe was assembled onto the gold nanoparticles. SEM (JSM-6330F, JEOL Co. Ltd., Beijing, China) showed the surface of graphene wrapped with the CMWCNT, and then the Au nanoparticles in the size range of 100 to 180 nm. The capture of the target DNA opened the hairpin and allowed the formation of a quadruplex with hemin that served as a DNAzyme to catalyze the  $\text{H}_2\text{O}_2$ -mediated oxidation of 3,3',5,5'-tetramethylbenzidine (TMB). Differential pulse voltammograms of the reduction of TMB gave a detection limit for the DNA segment, a specific sequence of the HBV X gene of  $0.5$  pM, and a linear range from  $10$  pM to  $10$  nM.

A composite nanostructured electrode was used to immobilize uricase and act as an amperometric sensor for uric acid [118]. Silver nanoparticles were first electrodeposited onto a gold rod electrode at  $-0.40$  V (versus Ag/AgCl) for 30 s from a solution of one mM of  $\text{AgNO}_3$  in  $0.2$  M of  $\text{KNO}_3$ . A membrane of chitosan and multiwalled carbon nanotubes was then electrospun onto the electrode. Using glutaraldehyde activation, uricase was immobilized through the amino groups of chitosan. Then, the enzyme electrode was used in a flow injection system. The reaction of uricase on uric acid consumes  $\text{O}_2$  and produces allantoin,  $\text{H}_2\text{O}_2$ , and  $\text{CO}_2$ . The electrode catalyzed the electroreduction of  $\text{O}_2$ , and the addition of uric acid resulted in a reduction of the reduction current. The change in reduction current was linear over the range one to  $400 \mu\text{M}$  of uric acid, and the detection limit was one  $\mu\text{M}$  when the sensor was operated at the optimal potential of  $-0.35$  V.

Composite nanostructures of MWCNT and clusters of gold nanoparticles were formed on GCE and used to make an amperometric  $\text{H}_2\text{O}_2$  sensor based on immobilized hemoglobin [119]. A dispersion of  $0.1 \text{ mg cm}^{-3}$  of MWCNT in toluene was drop cast onto a GCE, and then subjected to potential cycling from  $1.8$  V to  $-0.4$  V (versus Ag/AgCl) for 10 min in  $0.5$  M of  $\text{K}_2\text{SO}_4$  to introduce oxidized functional groups on defects in the MWCNT. Next, gold oxide complexes were formed on these sites by pulsing the potential from  $0.8$  V to  $1.5$  V, applying different pulse widths in a solution of  $0.1$  M of  $\text{HAuCl}_4$  in  $0.1$  M of  $\text{K}_2\text{SO}_4$ . The gold oxide clusters were converted to clusters of Au nanoparticles by cycling the potential from  $1.2$  V to  $-0.4$  V in  $0.1$  of  $\text{H}_2\text{SO}_4$ . Hemoglobin was immobilized from an  $80\text{-}\mu\text{M}$  solution by cycling the potential from  $-0.15$  V to  $1.15$  V at  $100 \text{ mV sec}^{-1}$  for 30 cycles. To complete the electrode modification, Nafion was solution cast over the surface. SEM (S-4800, Hitachi, Tokyo, Japan) revealed the occurrence of distinct clusters of Au nanoparticles along MWCNT. The pulse width that was used in the first step of the preparation influenced the nanoparticle size;  $0.0001$ -second pulses resulted in the formation of one nm of nuclei, which were converted into five-nm Au nanoparticles. Meanwhile,  $0.0005$ -second pulses resulted in formation of two-nm nuclei that were converted into  $10$ -nm Au nanoparticles, and  $0.001$ -second pulses resulted in formation of five-nm nuclei that were converted into  $50$ -nm Au nanoparticles. The direct electrochemistry of hemoglobin was observed, and a detection limit of  $0.2 \mu\text{M}$  and linear range from  $0.5$  to  $1000 \mu\text{M}$  was obtained from  $\text{H}_2\text{O}_2$ .

A carbon ionic liquid electrode was used for the electrodeposition of Au nanoparticles for the immobilization of myoglobin to make a direct electron transfer amperometric sensor for trichloroacetic acid or  $\text{H}_2\text{O}_2$  [120]. The compound 1-hexylpyridinium hexafluorophosphate and graphite powder was mixed into a paste, packed into a glass tube, and connected by a copper wire. Graphene sheets were electrodeposited from graphene oxide dispersion at  $-1.3$  V (versus SCE) for 600 s. The Au

nanoparticles were electrodeposited at  $-0.4$  V for 300 s from a solution of five mM of  $\text{HAuCl}_4$  and 0.5 M of  $\text{KNO}_3$ . Myoglobin was adsorbed, and then covered by a layer of Nafion. For  $\text{H}_2\text{O}_2$ , a detection limit of  $0.66 \mu\text{M}$  and a linear range from 1.98 to  $238.2 \mu\text{M}$  was found, and for trichloroacetic acid, a detection limit of 0.13 mM and a linear range from 0.4 to 20 mM was found.

Gold nanoparticles were electrodeposited onto GCE, but first they were surface modified with reduced graphene oxide sheets [121]. The electrodeposition at  $-0.2$  V (versus Ag/AgCl) from 0.3 mM of  $\text{HAuCl}_4$  produced Au nanoparticles decorating the petal-shaped graphene nanosize flakes. The decoration with Au nanoparticles doubled the effective surface area, which was determined using the Randles–Sevcik equation analysis and the  $\text{K}_4\text{Fe}(\text{CN})_6$  redox probe. The gold surfaces were modified with 2-(3,4-dihydroxy phenyl) benzothiazole, which promoted the electrocatalytic detection of levodopa, uric acid, and folic acid, whose peaks in square wave voltammetry sweeps were separated so that all three could be detected simultaneously.

A dispersion of exfoliated graphene oxide sheets and 0.5 mM of  $\text{HAuCl}_4$  was electrodeposited onto a GCE by scanning the potential (versus Ag/AgCl) to form a film of graphene sheets decorated with nanoparticles [122]. This electrode was found useful for the analysis of  $\text{CH}_3\text{Hg}^+$ , and the maximum response was for the electrode formed by five cycles of deposition. The detection limit was  $0.12 \mu\text{g mL}^{-1}$  as determined by DPV, and the electrode was useful for the detection of  $\text{CH}_3\text{Hg}^+$  in contaminated fish samples.

The electrodeposition of gold nanocubes onto a two-mm gold disk to which a thiolated graphene material had been fixed was used to make a third-generation glucose biosensor [123]. The deposition solution contained  $\text{HAuCl}_4$  and  $\text{KClO}_4$ . When a potential of  $-0.2$  V (versus Ag/AgCl) was used, 100-nm gold nanocubes were formed on the surface, and this structure was not observed at other potentials. Additionally, it was observed that if the total charge that passed exceeded five mC, then the morphology would begin to change from cube-like to denser flower-like nanostructures. Glucose oxidase was adsorbed onto the surface with the expectation that the thiol groups that projected from the graphene surface would undergo exchange with disulfide bridges in the enzyme. The sensor prepared on the gold nanocube-modified graphene showed the highest sensitivity of the morphologies examined, and gave a high sensitivity of  $221.0 \mu\text{A mmol L}^{-1} \text{cm}^{-2}$  at an operating potential of  $-0.4$  V (versus Ag/AgCl).

## 5.2. Composite Electrodes Containing Organic Polymers

Molecular imprinting combined with electrochemical deposition based on electrostatic interaction has been employed in the construction of a composite nanostructured electrode for electrochemical detection of glucose [124]. An amphiphilic random copolymer was used as a template for the molecular imprinting of glucose in organic solvent with the formation of polymer particles with an average diameter 100 nm, which was induced by the addition of water. Then, gold nanoparticles were formed by the direct reduction of  $\text{AuCl}_4^-$  by the pendant amino groups of the polymer. The imprinted polymer particles/Au nanoparticles composite was electrostatically immobilized on the surface of an Au electrode by the application of a  $-2.0$  V potential for two minutes. The glucose templates were extracted using acetic acid/methanol over a period of five days. The resulting modified electrode, with the use of  $[\text{Fe}(\text{CN})_6]^{3-/4-}$  as a probe, was found to be highly selective for glucose versus other sugars, as measured by the extent of current reduction in the presence of sugar.

A three-component layer of gold nanoparticles, nickel oxide nanoparticles, and conducting polymer was used for the covalent immobilization of tyrosinase to make an impedimetric sensor for dopamine [125]. Gold nanoparticles were first electrodeposited onto an ITO-coated glass electrode by applying 20 cycles between 0.1 V and  $-0.9$  V (versus Ag/AgCl) at  $50 \text{ mV sec}^{-1}$  in a one-mM solution of  $\text{HAuCl}_4$  with the resulting nanoparticles noted as having an average size of 74.49 nm. Next, nickel oxide nanoparticles were electrodeposited by applying 20 cycles between  $-1.2$  V and zero V at  $50 \text{ mV sec}^{-1}$  in a solution of 10 mM of  $\text{Ni}(\text{NO}_3)_2$ . The resulting NiO nanoparticles were on top of the gold nanoparticles, and were described as having an average diameter of 357.96 nm. Finally, on top

of the dual nanoparticle layer, a conducting polymer layer was formed by the electropolymerization of pyrrole propionic acid. The change in charge transfer resistance gave the sensor a linear range of 80  $\mu\text{M}$  to 0.20 mM with a detection limit of 5.46  $\mu\text{M}$ .

A composite film of gold nanoparticles and carboxymethyl- $\beta$ -cyclodextrins (CMCDs) was prepared by co-electrodeposition onto a GCE and used as a non-enzymatic glucose sensor [126]. Cyclic voltammetry scans were applied from  $-1.4$  to  $0.6$  V (versus Ag/AgCl) at  $100$   $\text{mV sec}^{-1}$  for two cycles in a solution of  $\text{HAuCl}_4$  and CMCD in pH 8.04 phosphate buffer. Cycling of the potential between  $-1.0$  V and  $1.0$  V at  $100$   $\text{mV sec}^{-1}$  was used to polymerize CMCDs. The presence of CMCDs resulted in a higher density of smaller gold nanoparticles on the GCE surface. The electrode showed electrocatalytic activity against a range of analytes, including dopamine, tyrosine, ascorbic acid, chloramphenicol, guanine, uric acid, thymine, and glucose. The performance as a non-enzymatic glucose sensor was evaluated by chronoamperometry at a potential of  $0.07$  V, and the response was 3.7 times greater for the composite-modified electrodes than for GCE modified with gold nanoparticles alone. The composite-modified electrode also had an extended linear range from  $0.001$  to  $110$  mM and a detection limit of  $0.99$   $\mu\text{M}$ .

The electropolymerization of aniline from a solution containing dispersed gold nanoparticles capped by polyvinylpyrrolidone resulted in a composite nanostructured film that was used as a support for glucose oxidase to make a glucose biosensor [127]. TEM images (Tecnai-12, Phillips, Eindhoven, Netherlands) showed that the PVP-capped gold nanoparticles were better dispersed than those that were uncapped. The film was electropolymerized onto a GCE by cycling the potential between  $-0.2$  and  $0.75$  V (versus SCE) at  $100$   $\text{mV sec}^{-1}$ . Glucose oxidase (eight  $\text{mg mL}^{-1}$ ) was drop cast onto the composite film, and then, a layer of Nafion was applied from a 0.5% solution. SEM (S-4800, Hitachi, Tokyo, Japan) images showed that the composite film had distinct flower-like structures. The immobilized glucose oxidase showed direct electron transfer and a limit of detection for glucose of  $1.0 \times 10^{-5}$  M.

The composite nanostructures of a conducting polymer and electrodeposited bimetallic Au–Pt nanoparticles were used as a support for HRP to make a  $\text{H}_2\text{O}_2$  sensor [128]. A polypyrrole film was deposited onto a GCE from a solution of  $0.05$  M of pyrrole in  $0.1$  M of  $\text{LiClO}_4$  by scanning from zero to one V (versus SCE). The bimetallic nanoparticles were electrodeposited at  $-0.2$  V from an equimolar solution of  $\text{HAuCl}_4$  and  $\text{H}_2\text{PtCl}_6$  in  $0.2$  M of  $\text{Na}_2\text{SO}_4$ . Subsequently, the nanoparticles surfaces were modified by immersion in a solution of L-cysteine for two hours. Calf thymus DNA was immobilized by electrostatic interaction, which was followed by the immobilization of HRP also by electrostatic immobilization. SEM (S-4800, Hitachi, Tokyo, Japan) revealed a high coverage of many globular nanoparticles. The detection of  $\text{H}_2\text{O}_2$  at  $-0.2$  V gave a detection limit of  $1.3$   $\mu\text{M}$  and a linear range from  $4.9$   $\mu\text{M}$  to  $4.8$  mM.

Gold nanoparticles were electrodeposited on SPCE and then modified with the enzyme cytochrome P450 2E1 electrostatically immobilized into a polyelectrolyte film of poly (diallyldimethylammonium chloride) (PDDA) and poly(sodium-p-styrenesulfonate) (PSS) [129]. The gold nanoparticles were formed on the SPCE from 1%  $\text{HAuCl}_4$  solution by applying a potential of  $-0.2$  V (versus Ag/AgCl) for 30 s. The enzyme-modified SPCE was used to detect 4-(methylnitrosamino)-1-(3-pyridyl)-1-butanone (NNK), which is a carcinogen formed in tobacco smoke. After electrodeposition, there was a fairly uniform distribution of  $\sim 100$ -nm gold nanoparticles over the SPCE surface of many irregular graphite particles. Application of the polyelectrolyte layer resulted in a smooth surface. The detection of NNK in urine using chronoamperometry with excellent recovery was demonstrated. SPCE substrates were also used as supports for composite electrodes of gold nanoparticles, laccase, and polypyrrole for the detection of polyphenols in propolis, which is the residue produced by honeybees [130]. The parameters for electrode preparation were all optimized in terms of the analytical response. Gold nanoparticles were electrodeposited at  $-400$  mV (versus Ag/AgCl) from 0.01%  $\text{HAuCl}_4$  in  $0.1$  M of KCl, resulting in particles that were 30 to 50 nm in size. Laccase was adsorbed by drop casting from  $10$   $\mu\text{g mL}^{-1}$  of solution. Pyrrole was electropolymerized from  $0.2$  M of pyrrole at  $700$  mV for 600 s, covering the enzyme with an

electroactive layer. The enzyme activity was at its maximum at pH 3.5, and with detection at  $-450$  mV in  $0.1$  M of acetate buffer of this pH, a detection limit of  $0.83$  mM was determined for polyphenols extracted from propolis using ethanol.

### 5.3. Composite Electrodes Containing Prussian Blue

Prussian blue (PB) is the compound known as  $(Fe_4^{III}[Fe^{II}(CN)_6]_3)$ , in which Fe(III) is coordinated to nitrogen, and Fe(II) is coordinated to carbon [131]. PB is known as an electrocatalyst for the oxidation of  $H_2O_2$ . Layer-by-layer modification of a GCE with PB and gold was used to make an amperometric sensor for  $H_2O_2$  [132].  $(PB-Au)_x$  multilayer films were made where  $x$  was varied from one to five. PB was electrodeposited first from a solution containing  $0.1$  M of  $K_2SO_4$ , one mM of  $K_3Fe(CN)_6$ , one mM of  $Fe_2(SO_4)_3$ , and  $0.05$  M of  $H_2SO_4$  by scanning the potential from one V to  $-0.2$  V (versus SCE) at  $50$  mV  $sec^{-1}$ . Gold was electrodeposited by scanning from  $0.65$  V to  $-0.2$  V at  $50$  mV  $sec^{-1}$  in a solution containing  $0.1$  M of  $K_2SO_4$ , one mM of  $HAuCl_4$ , and  $0.05$  M of  $H_2SO_4$ . The first step gave  $80$ -nm cubic-shaped PB nanoparticles that were visible in SEM (JEM-6700F, JEOL Co. Ltd., Beijing, China) and the second step gave gold nanoparticles of  $80$  nm (first layer) or  $100$  nm (second layer). A solution of glucose oxidase and dopamine was combined with  $Na_2PtCl_6$  and allowed to undergo the polymerization of dopamine to yield a dispersion of platinum nanoparticles and polydopamine, entrapping the enzyme glucose oxidase. Then, the dispersion was cast onto the electrode surface covered by  $(PB-Au)_2$ . The current response to glucose arising from the oxidation of  $H_2O_2$ , which was generated by the reaction, was monitored at  $-0.05$  V. A detection limit of  $0.5$   $\mu$ M and a linear range from  $0.008$  to  $0.79$  mM was found. Application to the determination of glucose in blood serum from healthy patients was successful.

A biosensor for  $Cu^{2+}$  based on a composite nanostructure containing a DNAzyme was formed by one-step electrodeposition [133]. The composite film was both three-dimensional and macroporous. Using vertical deposition, a layer of close-packed silica spheres was formed on a gold electrode. Then, single-walled carbon nanotubes were dispersed into a  $0.05\%$  (w/v) chitosan solution in  $1.0\%$  acetic acid. A second solution containing chitosan and the precursors to PB was prepared containing a solution with five mM of  $FeCl_3$ , five mM of  $K_3[Fe(CN)_6]$ ,  $0.2$  M of  $KCl$ ,  $0.2$  M of  $HCl$ , and  $10$  mL of  $0.05\%$  chitosan (CS). After combining these two solutions, electrodeposition onto the silica sphere-modified gold electrode was carried out at  $0.4$  V (versus SCE) for  $300$  s. Then, the silica template was dissolved away by brief treatment with  $5\%$  HF, leaving behind a macroporous film. The film was then scanned by CV between  $-0.05$  and  $0.35$  V at  $50$  mV  $sec^{-1}$  for  $25$  cycles, which resulted in the film becoming conductive. A dispersion of gold nanorods associated with graphene oxide and conjugated to enzymes glucose oxidase and HRP was then prepared. Gold nanorods were also conjugated to DNAzyme against  $Cu^{2+}$ , which resulted in the cleavage of DNA, whose association with a complimentary strand would then increase the current response to the enzymatic reduction of glucose. The sensor was highly selective for  $Cu^{2+}$  in the presence of other metal ions, and had a limit of detection of  $10^{-19}$  M.

A biosensor for  $\beta$ -glucan was made by immobilizing  $\beta$ -glucanase and glucose oxidase into a composite electrode containing PB nanoparticles, gold nanoparticles, and chitosan [134]. The  $H_2O_2$  produced by glucose oxidase, which underwent a reversible redox reaction with PB, was detected amperometrically at  $0.0$  V (versus Ag/AgCl) and a linear range from  $6.25$  to  $93.75$   $\mu$ M and a detection limit of  $1.56$   $\mu$ M. The first step for the construction of the nanocomposite electrode was to electrodeposit PB and chitosan from an aqueous solution of  $0.10$  M of  $KCl$ ,  $0.01$  M of  $HCl$ ,  $0.5$  mM of  $K_3[Fe(CN)_6]$ ,  $0.5$  mM of  $FeCl_3$  and  $0.01\%$  chitosan by cycling the potential from  $-0.1$  to  $0.45$  V at  $20$  mV  $sec^{-1}$  for  $10$  cycles to deposit the optimal thickness of the film on the gold disk electrode. Then, a layer of gold nanoparticles and chitosan was electrodeposited at  $-0.2$  V from a solution of  $0.1\%$   $HAuCl_4$  and  $0.025\%$  chitosan. SEM revealed  $50$ -nm sized nanocubes spread on the surface for the first layer, and after the second layer was deposited, Au nanoparticles that had dispersed within the chitosan were visible. The solution of both enzymes was drop cast on the surface, which was then followed by drying and cross-linking in glutaraldehyde. Figure 10 shows SEM images of the composite nanostructures,

along with CV scans of bare gold, PB, and chitosan (CS) on gold, gold nanoparticles with PB and chitosan on gold, and also with glucose oxidase ( $\beta$ -G-GOD) recorded in the presence of  $[\text{Fe}(\text{CN})_6]^{3-}$  and  $[\text{Fe}(\text{CN})_6]^{4-}$ , showing that the addition of PB and gold nanoparticles enhances electron transfer to and from the diffusing redox probe.

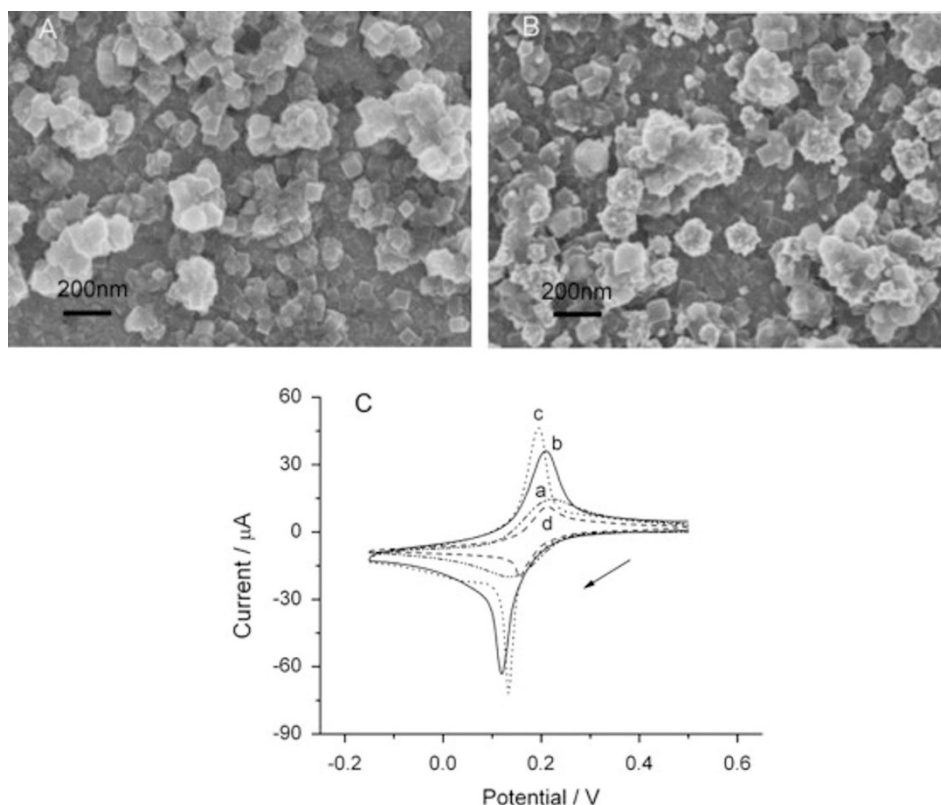


**Figure 10.** SEM images of Prussian blue and chitosan (PB-CS) nanocomposite film (A) and AuNPs-CS/PB-CS nanocomposite film (B). (C) Cyclic voltammograms (CVs) obtained from different modified electrodes in five mM of  $[\text{Fe}(\text{CN})_6]^{3-}/[\text{Fe}(\text{CN})_6]^{4-}$  containing 0.1 M of phosphate buffer solution (PBS) at a scan rate of  $20 \text{ mV s}^{-1}$ . (a) Bare Au, (b) PB-CS/Au, (c) AuNPs-CS/PB-CS/Au, and (d) CS/ $\beta$ -G-GOD/AuNPs-CS/PB-CS/Au electrode. Reproduced with permission from ref. [134], Copyright 2014, Elsevier.  $\beta$ -G-GOD: glucose oxidase.

#### 5.4. Composite Electrodes with Nafion

Nafion is a perfluorinated and sulfonated polymeric ionomer that can be cast over electrode surfaces to stabilize and entrap components while allowing for good ion exchange [135]. As such, it is promising for being cast over complex composite nanostructures on electrode surfaces. Gold nanoparticles were shown to be able to be electrodeposited into a Nafion membrane coating on either ITO glass or GCE [136]. The electrode surfaces were first covered by a solvent cast film of Nafion; then, electrodeposition proceeded at  $-0.2 \text{ V}$  (versus Ag/AgCl) from 1 wt%  $\text{HAuCl}_4$  in 0.5 M of  $\text{H}_2\text{SO}_4$  until a desired charge had passed. The deposition of the nanostructures was modified spectroelectrochemically following the emergence of the plasmon absorbance band. When a higher amount of charge passed, there were more nanoparticles that came closer together, and were often in contact with each other. The modified electrode was found to catalyze the oxidation of NO, which was generated in situ from  $\text{NaNO}_2$ , and a detection limit of one nM was observed.

#### 5.5. Composite Electrodes with Chitosan

Chitosan is the deacetylated form of natural chitin; it has excellent film-forming ability, is biocompatible, and is well-suited for the immobilization of enzymes [137]. A composite structure of

zirconia (ZrO)-coated SiO<sub>2</sub> nanoparticles and chitosan was formed on a gold electrode surface and used as the support for a lactate biosensor [138]. The modified electrode was formed by applying 20 potential cycles between  $-0.2$  to  $+0.4$  V in a suspension containing the nanoparticles in one M of KCl and 0.2% chitosan. Lactate oxidase was immobilized on this structure by cross-linking with glutaraldehyde. A linear relation between oxidation current and lactate concentration was observed over the range 0.1 to 4000 mM. The analytical recovery of lactate spiked into blood serum was noted as 96.6% to 99%. The biosensor was used to detect elevated lactate concentrations in patients with lactoacidosis.

A glucose sensor based on a composite film of gold nanoparticles, ionic liquid, and chitosan entrapping glucose oxidase was prepared using electrodeposition [139]. Gold nanoparticles with a size of 20 to 40 nm were deposited in 0.5 M of H<sub>2</sub>SO<sub>4</sub> and 10 mM of HAuCl<sub>4</sub> onto a gold surface by stepping the potential from 0.8 V to 0.2 V (versus Ag/AgCl) and then holding for 10 s. Then, a composite film containing glucose oxidase and chitosan was deposited from a solution of 0.5% chitosan, 20 mM of benzoquinone, 1% 1-butyl-3-methyl-imidazolium tetrafluoroborate (BMIM·BF<sub>4</sub>) as the ionic liquid and 5.0 mg mL<sup>-1</sup> of glucose oxidase. The benzoquinone served as a proton trap that increased the pH near the gold surface, thus leading to the deprotonation of chitosan and its deposition. In the final step, a layer of Nafion was cast over the composite film. Glucose was detected via the amperometric detection of H<sub>2</sub>O<sub>2</sub> at 0.6 V with a detection limit of 1.5 μM and a linear range from three μM to nine mM.

A non-enzymatic glucose sensor was prepared by one-step electrodeposition from a solution of HAuCl<sub>4</sub> and chitosan in 0.5 M of acetic acid onto a GCE electrode [140]. The electrodeposition took place at  $-1.0$  V (versus SCE) for 60 s, producing a film of Au nanoparticles in a chitosan film. For the optimized conditions, the detection limit for glucose detection was 0.37 mM with a linear range from 0.4 to 10.7 mM, which was based on the peak currents in the cyclic voltammograms in 0.10 M of NaOH.

### 5.6. Composite Electrodes with Silica

A sensor for superoxide was made by electrodepositing Au nanoparticles on ITO glass, and then modifying them with cysteine and superoxide dismutase in a silica gel layer [141]. The Au nanoparticles were deposited by cyclic voltammetry between  $-0.2$  V and  $-1.3$  V for 20 cycles at 50 mV sec<sup>-1</sup> in 0.1 mM of KAu(CN)<sub>2</sub> in 0.05 M of pH 7.5 phosphate buffer. The Au nanoparticles had an average size of 28 nm. Then, the Au nanoparticle-coated ITO glass was immersed into a solution of superoxide dismutase, cysteine, and silica gel. The direct electron transfer of superoxide dismutase was observed by cyclic voltammetry, and the peak current increased for up to 20 cycles of electrodeposition, which was used to form the nanoparticles. Superoxide was generated by the reaction of DMSO and NaOH. A linear response to superoxide was observed over the range of 0.08 to 0.64 μM. In an earlier report, for which the silica gel layer was not included, a coverage of enzymes of  $1.04 \times 10^{-10}$  mol cm<sup>-2</sup> was estimated [142].

The performance of glucose oxidase immobilized on electrodeposited Au, CdS, or ZnS nanoparticles on ITO glass and covered by a silica layer were compared [143]. The Au nanoparticles were deposited from 0.2 mM of HAuCl<sub>4</sub> in 0.02 M of pH 7 buffer by applying 20 cycles between 0.1 V and  $-0.9$  V (versus SCE) at 50 mV sec<sup>-1</sup>. Cadmium sulfide nanoparticles were deposited by applying 40 potential cycles between  $-0.4$  V and  $-0.8$  V at 50 mV sec<sup>-1</sup> at 50 °C in 0.8 mM of Na<sub>2</sub>S<sub>2</sub>O<sub>3</sub> and 0.05 M of CdCl<sub>2</sub> at pH 2–3. Zinc sulfide nanoparticles were prepared by applying 40 cycles at 50 °C between  $-0.4$  V and  $-1.0$  V at 50 mV sec<sup>-1</sup> from 0.8 mM of Na<sub>2</sub>S<sub>2</sub>O<sub>3</sub> and 0.05 M of ZnCl<sub>2</sub> at pH 4. Then, the solution of glucose oxidase and silica sol and polyvinyl alcohol was deposited over the nanoparticles. It was found that the electroactivity of the glucose oxidase was greatest on ZnS nanoparticles, and that these sensors also showed the greatest sensitivity to glucose.

## 6. Comparison of the Advantages and Performance of Different Nanostructures

The research reported to date involves many kinds of nanostructures, which were prepared under a variety of conditions on different sizes and types of electrodes, and addressing different analytical targets using different methods of measurement. Some of the studies concern the same or similar



analytical target measured using the same technique. It is important to consider the question of which structures appear to be providing the most promising limits of detection (generally reported for  $S/N = \text{three}$ ) and linear range, amongst other analytical parameters such as the stability of the response over time. Across all of the studies, analytical parameters are not necessarily reported in the same format. However, it is possible to make some comparisons for analytes, which have been the subject of multiple studies, such as sensors using glucose oxidase with direct electrochemical detection, sensors for non-enzymatic glucose detection, the detection of glucose-based on the detection of  $H_2O_2$  generated by the action of glucose oxidase, and DNA hybridization sensors. For the case of DNA hybridization, oligonucleotide length is a complicating factor, as is the use of different detection methods. Other studies may concern an analyte that has only been studied once or a few times using an electrochemically-deposited nanostructure, and are thus not able to be used in comparisons.

A significant fraction of studies concern the detection of  $H_2O_2$ , which is usually because it is produced by the action of the enzyme glucose oxidase in an effort to make a first-generation glucose sensor. Almost all of these studies report the performance of the sensor in terms of the response to glucose. One study did report both the response to  $H_2O_2$  concentration and the response to glucose concentration [123], finding them to be slightly different (detection limit of  $0.9 \mu\text{M}$  for  $H_2O_2$  alone versus a detection limit of  $0.5 \mu\text{M}$  for glucose). A desirable outcome would clearly be both a low limit of detection and a wide linear range. Many of the reports cite detection limits for glucose, as detected by the  $H_2O_2$  resulting from glucose oxidase action, in the low micromolar range. The most promising results in this case appear to have been found for some of the composite nanostructured films, providing some motivation for the appeal of developing these more complex electrodeposited structures in which different components may act together synergistically. The limit of detection of  $0.02 \mu\text{M}$  and linear range from  $2 \mu\text{M}$  to  $5.5 \text{mM}$  that was reported for the composite structure that was previously described [103] is impressive. The result of a limit of detection of  $0.21 \mu\text{M}$  and two linear ranges extending up to  $16.8 \text{mM}$  [105] is also noteworthy, although it is not clear why two distinct linear ranges occur. Some studies have reported the detection of  $H_2O_2$  by direct electron transfer between immobilized HRP and the electrode surface [13,21,25], and the results for HRP physisorbed on gold nanoparticles on ITO glass seem most attractive, offering both a low limit of detection of  $2 \mu\text{M}$  and an extended linear range of up to  $30 \text{mM}$ . As has been proposed [1], sensors working on direct electron transfer require minimizing the distance between enzyme active sites and the gold nanoparticle or nanostructure surface.

The electrochemical response to glucose alone without enzymes on the nanostructured electrode is the aim of 'non-enzymatic' glucose sensing, of which some examples have been described above. Of the reported studies, the result of a limit of detection of  $2.1 \mu\text{M}$  and an extended linear range from  $5 \mu\text{M}$  to  $16.4 \text{mM}$  on gold nanotube arrays is outstanding, and suggests that the access of glucose in solution to these regularly ordered structures of high surface area can be a promising principle for this and related sensors [48]. However, again, a composite nanostructure has proven highly impressive for non-enzymatic glucose sensing, with the composite of gold nanoparticles and polymerized cyclodextrin providing an extended linear range of up to  $110 \text{mM}$ , and a low detection limit of  $0.99 \mu\text{M}$  [118].

Almost all of the reported studies concerning the detection of a complimentary DNA strand by hybridization with an immobilized probe DNA strand concern the use of forms of electrodeposited gold with a high surface to volume ratio such as gold nanotubes [53,60], dendritic gold [73], other ramified forms of gold [84–86], and varied morphologies of electrodeposited platinum [92–94]. The length of the complimentary DNA strands studied varies from 20-mers [91–93] to as long as 41-mers [73]. The binding affinity of complimentary DNA strands increases with length, but also depends on sequence [144]. Comparisons of the detection for different strand lengths will be complicated by this dependence. Methods of detection also vary, but methylene blue as a redox probe that shows differential binding between single and double-stranded DNA has been used in multiple studies with either DPV or square wave voltammetry detection. Detection limits in the range of  $18 \text{zM}$  (zeptomolar,

$10^{-21}$  M) [86], 31 zM [84], and 47 zM [85] reported for 24-mer, 29-mer, and 25-mer complimentary strands, respectively, are most impressive. These results were obtained using structure-directing agents during electrodeposition to produce highly anisotropic or leaf-like gold deposits. Thus, it seems that highly ramified structures of gold that can allow oligonucleotide strands to project well out into solution without crowding are a superior direction for the further development of DNA sensors based on electrodeposited nanostructures.

## 7. Conclusions

The area of developing biosensors based on electrodeposited nanostructures has many possible applications to the detection of small molecules, metabolites, protein antigens, oligonucleotides, and other targets, including bacteria and viruses. The variety of substrate electrodes and preparation conditions can produce a vast range of structures. Many additional targets of high interest for the development of diagnostics such as glycoproteins, circulating tumor cells, circulating oligonucleotides, microRNAs, and content in microvesicles remain to be explored. As the work reported thus far covers both many different structures and many different targets, an area for future focus could be the identification of the optimal nanostructure for use with a specified target or class of targets. Further understanding of the relation of electrodeposition parameters and the resulting structures is needed. Additionally, for practical application of these electrodes, further study of the stability and integration into practical devices will be required in the future.

**Funding:** The author acknowledges National Institutes of Health grant GM111835.

**Conflicts of Interest:** The author declares no conflict of interest.

## References

1. Taurino, I.; Sanzò, G.; Antiochia, R.; Tortolini, C.; Mazzei, F.; Favero, G.; De Micheli, G.; Carrara, S. Recent advances in third generation biosensors based on Au and Pt nanostructured electrodes. *Trends Anal. Chem.* **2016**, *79*, 151–159. [[CrossRef](#)]
2. Bhattarai, J.; Neupane, D.; Nepal, B.; Mikhaylov, V.; Demchenko, A.V.; Stine, K.J. Preparation, modification, characterization, and biosensing application of nanoporous gold using electrochemical techniques. *Nanomaterials* **2018**, *8*, 171. [[CrossRef](#)] [[PubMed](#)]
3. Stine, K.J. Enzyme immobilization on nanoporous gold—A review. *Biochem. Insights* **2017**, *10*, 1–12. [[CrossRef](#)] [[PubMed](#)]
4. Kyaw, H.H.; Al-Harhi, S.H.; Sellai, A.; Dutta, J. Self-organization of gold nanoparticles on silanated surfaces. *Beilstein J. Nanotechnol.* **2015**, *6*, 2345–2353. [[CrossRef](#)] [[PubMed](#)]
5. Haddada, M.B.; Blanchard, J.; Casale, S.; Krafft, J.-M.; Vallée, A.; Méthivier, C.; Boujday, S. Optimizing the immobilization of gold nanoparticles on functionalized silicon surfaces: Amine- vs thiol-terminated silane. *Gold Bull.* **2013**, *46*, 335–341. [[CrossRef](#)]
6. Yu, H.; Zhu, Y.; Yang, H.; Nakanishi, K.; Kanamori, K.; Guo, X. Facile preparation of silver nanoparticles homogeneously immobilized in hierarchically monolithic silica using ethylene glycol as reductant. *Dalton Trans.* **2014**, *43*, 12648–12656. [[CrossRef](#)] [[PubMed](#)]
7. Taglietti, A.; Arciola, C.R.; D'Agostino, A.; Dacarro, G.; Montanaro, L.; Campoccia, D.; Cucca, L.; Vercellino, M.; Poggi, A.; Pallavicini, P.; et al. Antibiofilm activity of a monolayer of silver nanoparticles anchored to an amino-silanized glass surface. *Biomaterials* **2014**, *35*, 1779–1788. [[CrossRef](#)] [[PubMed](#)]
8. Yáñez-Sedeño, P.; Pingarrón, J.M. Gold nanoparticle-based electrochemical biosensors. *Anal. Bioanal. Chem.* **2005**, *382*, 884–886. [[CrossRef](#)] [[PubMed](#)]
9. Chikae, M.; Idegami, K.; Kerman, K.; Nagatani, N.; Ishikawa, M.; Takamura, Y.; Tamiya, E. Direct fabrication of catalytic metal nanoparticles onto the surface of a screen-printed carbon electrode. *Electrochem. Commun.* **2006**, *8*, 1375–1380. [[CrossRef](#)]
10. Song, Y.; Ma, Y.; Di, J.; Tu, Y. Electrochemical deposition of gold–platinum alloy nanoparticles on an indium tin oxide electrode and their electrocatalytic applications. *Electrochim. Acta* **2010**, *55*, 4909–4914. [[CrossRef](#)]

11. Newman, J.D.S.; Blanchard, G.J. Formation of Gold Nanoparticles Using Amine Reducing Agents. *Langmuir* **2006**, *22*, 5882–5887. [[CrossRef](#)] [[PubMed](#)]
12. McCreery, R.L. Advanced Carbon Electrode Materials for Molecular Electrochemistry. *Chem. Rev.* **2008**, *108*, 2646–2687. [[CrossRef](#)] [[PubMed](#)]
13. Haghshenas, E.; Madrakian, T.; Afkhami, A.; Nabiabad, H.S. A label-free electrochemical biosensor based on tubulin immobilized on gold nanoparticle/glassy carbon electrode for the determination of vinblastine. *Anal. Bioanal. Chem.* **2017**, *409*, 5269–5278. [[CrossRef](#)] [[PubMed](#)]
14. Hernández-Cancel, G.; Suazo-Dávila, D.; Medina-Guzmán, J.; Rosado-González, M.; Díaz-Vázquez, L.M.; Griebenow, K. Chemically glycosylation improves the stability of an amperometric horseradish peroxidase biosensor. *Anal. Chim. Acta* **2015**, *854*, 129–139. [[CrossRef](#)] [[PubMed](#)]
15. Dimcheva, N.; Horozova, E.; Ivanov, Y.; Godjevargova, T. Self-assembly of acetylcholinesterase on gold nanoparticles electrodeposited on graphite. *Cent. Eur. J. Chem.* **2013**, *11*, 1740–1748. [[CrossRef](#)]
16. Yang, S.; Ding, S.; Li, L.; Ding, S.; Cao, Q.; Yang, J.; Xu, W.; Chen, A. One-Step Preparation of Direct Electrochemistry HRP Biosensor via Electrodeposition. *J. Electrochem. Soc.* **2017**, *164*, B710–B714. [[CrossRef](#)]
17. Guo, Y.; Wang, X.; Sun, X. A label-free electrochemical aptasensor based on electrodeposited gold nanoparticles and methylene blue for tetracycline detection. *Int. J. Electrochem. Sci.* **2015**, *10*, 3668–3679.
18. Yin, H.; Wang, X.; Guo, Y.; Zhou, Y.; Ai, S. Electrochemical detection of protein kinase activity based on carboxypeptidase Y digestion triggered signal amplification. *Biosens. Bioelectron.* **2015**, *66*, 77–83. [[CrossRef](#)] [[PubMed](#)]
19. El-Said, W.A.; Lee, J.-H.; Oh, B.-K.; Choi, J.-W. 3-D nanoporous gold thin film for the simultaneous electrochemical determination of dopamine and ascorbic acid. *Electrochem. Commun.* **2010**, *12*, 1756–1759. [[CrossRef](#)]
20. Bhattarai, J.K.; Sharma, A.; Fujikawa, K.; Demchenko, A.V.; Stine, K.J. Electrochemical synthesis of nanostructured gold film for the study of carbohydrate–lectin interactions using localized surface plasmon resonance spectroscopy. *Carbohydr. Res.* **2015**, *405*, 55–65. [[CrossRef](#)] [[PubMed](#)]
21. Wang, Y.; Deng, J.; Di, J.; Tu, J. Electrodeposition of large size gold nanoparticles on indium tin oxide glass and application as refractive index sensor. *Electrochem. Commun.* **2009**, *11*, 1034–1037. [[CrossRef](#)]
22. Bollella, P.; Gorton, L.; Ludwig, R.; Antiochia, R. A third generation glucose biosensor based on cellobiose dehydrogenase immobilized on a glassy carbon electrode decorated with electrodeposited gold nanoparticles: Characterization and Application in Human Saliva. *Sensors* **2017**, *17*, 1912. [[CrossRef](#)] [[PubMed](#)]
23. Gao, W.; Zhang, A.; Chen, Y.; Chen, Z.; Chen, Y.; Lu, F.; Chen, Z. A novel probe density controllable electrochemiluminescence biosensor for ultra-sensitive detection of Hg<sup>2+</sup> based on DNA hybridization optimization with gold nanoparticles array patterned self-assembly platform. *Biosens. Bioelectron.* **2013**, *49*, 139–145. [[CrossRef](#)] [[PubMed](#)]
24. Wu, Z.; Chen, L.; Shen, G.; Yu, R. Platinum nanoparticle-modified carbon fiber ultramicroelectrodes for mediator-free biosensing. *Sens. Actuators B* **2006**, *119*, 295–301. [[CrossRef](#)]
25. Zhao, F.; Xie, Q.; Xu, M.; Wang, S.; Zhou, J.; Liu, F. RNA aptamer based electrochemical biosensor for sensitive and selective detection of cAMP. *Biosens. Bioelectron.* **2015**, *66*, 238–243. [[CrossRef](#)] [[PubMed](#)]
26. Wang, D.; Dou, W.; Zhao, G.; Chen, Y. Immunosensor based on electrodeposition of gold-nanoparticles and ionic liquid composite for detection of *Salmonella pullorum*. *J. Microbiol. Methods* **2014**, *106*, 110–118. [[CrossRef](#)] [[PubMed](#)]
27. Aydın, E.B.; Sezgintürk, M.K. Indium tin oxide (ITO): A promising material in biosensing technology. *Trends Anal. Chem.* **2017**, *97*, 309–315. [[CrossRef](#)]
28. Wang, J.; Wang, L.; Di, J.; Tu, Y. Electrodeposition of gold nanoparticles on indium/tin oxide electrode for fabrication of a disposable hydrogen peroxide biosensor. *Talanta* **2009**, *77*, 1454–1459. [[CrossRef](#)] [[PubMed](#)]
29. Zhao, Y.; Wu, Y.; Zhang, Y.; Chen, Z.; Cao, X.; Di, J.; Yang, J. Electrocatalytic behavior and amperometric detection of morphine on ITO electrode modified with directly electrodeposited gold nanoparticles. *Electroanalysis* **2009**, *21*, 939–943. [[CrossRef](#)]
30. Deng, J.; Song, Y.; Wang, Y.; Di, J. Label-free optical biosensor based on localized surface plasmon resonance of twin-linked gold nanoparticles electrodeposited on ITO glass. *Biosens. Bioelectron.* **2010**, *26*, 615–619. [[CrossRef](#)] [[PubMed](#)]
31. Chen, H.; Shao, L.; Lia, Q.; Wang, J. Gold nanorods and their plasmonic properties. *Chem. Soc. Rev.* **2013**, *42*, 2679–2724. [[CrossRef](#)] [[PubMed](#)]

32. Hu, Y.; Song, Y.; Wang, Y.; Di, J. Electrochemical synthesis of gold nanoparticles onto indium tin oxide glass and application in biosensors. *Thin Solid Films* **2011**, *519*, 6605–6609. [[CrossRef](#)]
33. Deng, J.; Du, J.; Wang, Y.; Tu, Y.; Di, J. Synthesis of ultrathin silver shell on gold core for reducing substrate effect of LSPR sensor. *Electrochem. Commun.* **2011**, *13*, 1517–1520. [[CrossRef](#)]
34. Dong, P.; Lin, Y.; Deng, J.; Di, J. Ultrathin gold-shell coated silver nanoparticles onto a glass platform for improvement of plasmonic sensors. *ACS Appl. Mater. Interfaces* **2013**, *5*, 2392–2399. [[CrossRef](#)] [[PubMed](#)]
35. Ma, Y.; Di, J.; Yan, X.; Zhao, M.; Lu, Z.; Tu, Y. Direct electrodeposition of gold nanoparticles on indium tin oxide surface and its application. *Biosens. Bioelectron.* **2009**, *24*, 1480–1483. [[CrossRef](#)] [[PubMed](#)]
36. Zhang, K.; Wei, J.; Zhu, H.; Ma, F.; Wang, S. Electrodeposition of gold nanoparticle arrays on ITO glass as electrode with high electrocatalytic activity. *Mater. Res. Bull.* **2013**, *48*, 1338–1341. [[CrossRef](#)]
37. Ahmad, M.; Pan, C.; Gan, L.; Nawaz, Z.; Zhu, J. Highly Sensitive Amperometric Cholesterol Biosensor Based on Pt-Incorporated Fullerene-like ZnO Nanospheres. *J. Phys. Chem. C* **2010**, *114*, 243–250. [[CrossRef](#)]
38. Ahmadzadeh-Raji, M.; Ghafar-Zadeh, E.; Amoabediny, G. An optically-transparent aptamer-based detection system for colon cancer applications using gold nanoparticles electrodeposited on indium tin oxide. *Sensors* **2016**, *16*, 1071. [[CrossRef](#)] [[PubMed](#)]
39. Li, L.; Zhai, T.; Zeng, H.; Fang, X.; Bando, X.; Golberg, D. Polystyrene sphere-assisted one-dimensional nanostructure arrays: Synthesis and applications. *J. Mater. Chem.* **2011**, *21*, 40–56. [[CrossRef](#)]
40. Bartlett, P.N.; Baumberg, J.J.; Birkin, P.R.; Ghanem, M.A.; Netti, M.C. Highly ordered macroporous gold and platinum films formed by electrochemical deposition through templates assembled from submicron diameter monodisperse polystyrene spheres. *Chem. Mater.* **2002**, *14*, 2199–2208. [[CrossRef](#)]
41. Bartlett, P.N.; Birkin, P.R.; Ghanem, M.A. Electrochemical deposition of macroporous platinum, palladium and cobalt films using polystyrene latex sphere templates. *Chem. Commun.* **2000**, *17*, 1671–1672. [[CrossRef](#)]
42. Kinkead, B.; van Druenen, J.; Paul, M.T.Y.; Dowling, K.; Jerkiewicz, G.; Gates, B.D. Platinum ordered porous electrodes: Developing a platform for fundamental electrochemical characterization. *Electrocatalysis* **2013**, *4*, 179–186. [[CrossRef](#)]
43. Wang, J.; Duan, G.; Liu, G.; Li, Y.; Dai, Z.; Zhang, H.; Cai, W. Gold quasi rod-shaped nanoparticle-built hierarchically micro/nanostructured pore array via clean electrodeposition on a colloidal monolayer and its structurally enhanced SERS performance. *J. Mater. Chem.* **2011**, *21*, 8816–8821. [[CrossRef](#)]
44. Wang, C.; Yang, C.; Song, Y.; Gao, W.; Xia, X. Adsorption and direct electron transfer from hemoglobin into a three-dimensionally ordered macroporous gold film. *Adv. Funct. Mater.* **2005**, *15*, 1267–1275. [[CrossRef](#)]
45. Laviron, E.A. The use of linear potential sweep voltammetry and of a.c. voltammetry for the study of the surface electrochemical reaction of strongly adsorbed systems and of redox modified electrodes. *J. Electroanal. Chem. Interfacial Electrochem.* **1979**, *100*, 263–270. [[CrossRef](#)]
46. Cho, K.; Loget, G.; Corn, R.M. Lithographically patterned nanoscale electrodeposition of plasmonic, bimetallic, semiconductor, magnetic, and polymer nanoring arrays. *J. Phys. Chem. C* **2014**, *118*, 28993–29000. [[CrossRef](#)] [[PubMed](#)]
47. Toma, M.; Cho, K.; Wood, J.B.; Corn, R.M. Gold nanoring arrays for near infrared plasmonic biosensing. *Plasmonics* **2014**, *9*, 765–772. [[CrossRef](#)]
48. Clark, A.W.; Glidle, A.; Cumming, D.R.S.; Cooper, J.M. Plasmonic split-ring resonators as dichroic nanophotonic DNA biosensors. *J. Am. Chem. Soc.* **2009**, *131*, 17615–17619. [[CrossRef](#)] [[PubMed](#)]
49. Halpern, A.R.; Corn, R.M. Lithographically patterned electrodeposition of gold, silver, and nickel nanoring arrays with widely tunable near-infrared plasmonic resonances. *ACS Nano* **2013**, *7*, 1755–1762. [[CrossRef](#)] [[PubMed](#)]
50. Thormann, A.; Teuscher, N.; Pfannmüller, M.; Rothe, U.; Heilmann, A. Nanoporous aluminum oxide membranes for filtration and biofunctionalization. *Small* **2007**, *3*, 1032–1040. [[CrossRef](#)] [[PubMed](#)]
51. Itaya, K.; Sugawara, S.; Arai, K.; Saito, S. Properties of porous anodic aluminum oxide films as membranes. *J. Chem. Eng. Jpn.* **1984**, *17*, 514–520. [[CrossRef](#)]
52. Poinern, G.E.J.; Ali, N.; Fawcett, D. Progress in nano-engineered anodic aluminum oxide membrane development. *Materials* **2011**, *4*, 487–526. [[CrossRef](#)] [[PubMed](#)]
53. Tian, T.; Dong, J.; Xu, J. Direct electrodeposition of highly ordered gold nanotube arrays for use in non-enzymatic amperometric sensing of glucose. *Microchim. Acta* **2016**, *183*, 1925–1932. [[CrossRef](#)]

54. Hui, J.; Cui, J.; Wang, Y.; Zhang, Y.; Liang, J.; Zhang, X.; Chen, W.; Ogabiela, E.E.; Adeloju, S.B.; Wu, Y. A high throughput glucose biosensor based on FIA and gold nanowire arrays at low potential. *J. Electrochem. Soc.* **2014**, *161*, B291–B296. [[CrossRef](#)]
55. Yuan, J.; Wang, K.; Xia, X. Highly ordered platinum-nanotubule arrays for amperometric glucose sensing. *Adv. Funct. Mater.* **2005**, *15*, 803–809. [[CrossRef](#)]
56. Takahashia, Y.; Tatsuma, T. Electrodeposition of thermally stable gold and silver nanoparticle ensembles through a thin alumina nanomask. *Nanoscale* **2010**, *2*, 1494–1499. [[CrossRef](#)] [[PubMed](#)]
57. Kuemmel, M.; Allouche, J.; Nicole, L.; Boissière, C.; Laberty, C.; Amenitsch, H.; Sanchez, C.; Grosso, D. A chemical solution deposition route to nanopatterned inorganic material surfaces. *Chem. Mater.* **2007**, *19*, 3717–3725. [[CrossRef](#)]
58. Torati, S.R.; Reddy, V.; Yoon, S.S.; Kim, C. Electrochemical biosensor for *Mycobacterium tuberculosis* DNA detection based on gold nanotubes array electrode platform. *Biosens. Bioelectron.* **2016**, *78*, 483–488. [[CrossRef](#)] [[PubMed](#)]
59. Ramulu, T.S.; Venu, R.; Sinha, B.; Lim, B.; Jeon, S.J.; Yoon, S.S.; Kim, C.G. Nanowires array modified electrode for enhanced electrochemical detection of nucleic acid. *Biosens. Bioelectron.* **2013**, *40*, 258–264. [[CrossRef](#)] [[PubMed](#)]
60. Shariati, M.; Ghorbani, M.; Sasanpour, P.; Karamizefreh, A. An ultrasensitive label free human papilloma virus DNA biosensor using gold nanotubes based on nanoporous polycarbonate in electrical alignment. *Anal. Chim. Acta* **2019**, *1048*, 31–41. [[CrossRef](#)] [[PubMed](#)]
61. Yi, X.; Wu, Y.; Tan, G.; Yu, P.; Zhou, L.; Zhou, Z.; Chen, J.; Wang, Z.; Pang, J.; Ning, C. Palladium nanoparticles entrapped in a self-supporting nanoporous gold wire as sensitive dopamine biosensor. *Sci. Rep.* **2017**, *7*, 7941. [[CrossRef](#)] [[PubMed](#)]
62. Wang, D.; Tan, Y. Electrodeposition of enzymes-integrated mesoporous composite films by interfacial templating: A paradigm for electrochemical biosensors. *Electrochim. Acta* **2014**, *116*, 495–503. [[CrossRef](#)]
63. Leonardo, S.; Garibo, D.; Fernández-Tejedor, M.; O’Sullivan, C.K.; Campàs, M. Addressed immobilization of biofunctionalized diatoms on electrodes by gold electrodeposition. *Biofabrication* **2017**, *9*, 015027. [[CrossRef](#)] [[PubMed](#)]
64. Kim, S.H.; Nam, O.; Jin, E.; Gu, M.B. A new coccolith modified electrode-based biosensor using a cognate pair of aptamers with sandwich-type binding. *Biosens. Bioelectron.* **2019**, *123*, 160–166. [[CrossRef](#)] [[PubMed](#)]
65. Pippa, N.; Dokoumetzidis, A.; Demetzos, C.; Macheras, P. On the ubiquitous presence of fractals and fractal concepts in pharmaceutical sciences: A review. *Int. J. Pharm.* **2013**, *456*, 340–352. [[CrossRef](#)] [[PubMed](#)]
66. Meng, G.; Paulose, J.; Nelson, D.R.; Manoharan, V.N. Elastic instability of a crystal growing on a curved surface. *Science* **2014**, *343*, 634–637. [[CrossRef](#)] [[PubMed](#)]
67. Fransaer, J.L.; Penner, R.M. Brownian dynamics simulation of the growth of metal nanocrystal ensembles on electrode surfaces from solution. I. instantaneous nucleation and diffusion-controlled growth. *J. Phys. Chem. B* **1999**, *103*, 7643–7653. [[CrossRef](#)]
68. Drews, T.O.; Radisic, A.; Erlebacher, J.; Braatz, R.D.; Searson, P.C.; Alkire, R.C. Stochastic simulation of the early stages of kinetically limited electrodeposition. *J. Electrochem. Soc.* **2006**, *153*, C434–C441. [[CrossRef](#)]
69. Hill, H.D.; Millstone, J.E.; Banholzer, M.J.; Mirkin, C.A. The role radius of curvature plays in thiolated oligonucleotide loading on gold nanoparticles. *ACS Nano* **2009**, *3*, 418–424. [[CrossRef](#)] [[PubMed](#)]
70. Lin, T.H.; Lin, C.-W.; Liu, H.-H.; Sheu, J.-T.; Hung, W.-H. Potential-controlled electrodeposition of gold dendrites in the presence of cysteine. *Chem. Commun.* **2011**, *47*, 2044–2046. [[CrossRef](#)] [[PubMed](#)]
71. Nazari-Vanania, R.; Sattarahmady, N.; Yadegari, H.; Helia, H. A novel and ultrasensitive electrochemical DNA biosensor based on an ice crystals-like gold nanostructure for the detection of *Enterococcus faecalis* gene sequence. *Colloids Surf. B Biointerfaces* **2018**, *166*, 245–253. [[CrossRef](#)] [[PubMed](#)]
72. Hau, N.Y.; Yang, P.; Liu, C.; Wang, J.; Lee, P.-H.; Feng, S.-P. Aminosilane-assisted electrodeposition of gold nanodendrites and their catalytic properties. *Sci. Rep.* **2017**, *7*, 39839. [[CrossRef](#)] [[PubMed](#)]
73. Heli, H.; Amirizadeh, O. Non-enzymatic glucose biosensor based on hyperbranched pine-like gold nanostructure. *Mater. Sci. Eng. C* **2016**, *63*, 150–154. [[CrossRef](#)] [[PubMed](#)]
74. Shen, D.; Liu, Y.; Fang, Y.; Li, P.; Yang, Z. A sensor for glycoproteins based on dendritic gold nanoparticles electrodeposited on a gold electrode and modified with a phenylboronic acid. *J. Solid State Electrochem.* **2015**, *19*, 563–568. [[CrossRef](#)]

75. Jung, H.; Lee, S.H.; Yang, J.; Cho, M.; Lee, Y. Ni(OH)<sub>2</sub>@Cu dendrite structure for highly sensitive glucose determination. *RSC Adv.* **2014**, *4*, 47714–47720. [[CrossRef](#)]
76. Wu, L.; Zhang, X.; Chen, J. A new third-generation biosensor for superoxide anion based on dendritic gold nanostructure. *J. Electroanal. Chem.* **2014**, *726*, 112–118. [[CrossRef](#)]
77. Chen, Y.; Yang, X.-J.; Guo, L.-R.; Li, J.; Xia, X.-H.; Zheng, L.-M. Direct electrochemistry and electrocatalysis of hemoglobin at three-dimensional gold film electrode modified with self-assembled monolayers of 3-mercaptopropylphosphonic acid. *Anal. Chim. Acta* **2009**, *644*, 83–89. [[CrossRef](#)] [[PubMed](#)]
78. Shu, H.; Cao, L.; Chang, G.; He, H.; Zhang, Y.; He, Y. Direct electrodeposition of gold nanostructures onto glassy carbon electrodes for non-enzymatic detection of glucose. *Electrochim. Acta* **2014**, *132*, 524–532. [[CrossRef](#)]
79. Qiu, R.; Zhang, X.L.; Qiao, R.; Li, Y.; Kim, Y.; Kang, Y.S. CuNi dendritic material: Synthesis, mechanism discussion, and application as glucose sensor. *Chem. Mater.* **2007**, *19*, 4174–4180. [[CrossRef](#)]
80. Tanga, J.; Tang, D.; Niessner, R.; Knopp, D.; Chen, G. Hierarchical dendritic gold microstructure-based aptasensor for ultrasensitive electrochemical detection of thrombin using functionalized mesoporous silica nanospheres as signal tags. *Anal. Chim. Acta* **2012**, *720*, 1–8. [[CrossRef](#)] [[PubMed](#)]
81. Shi, L.; Chu, Z.; Liu, Y.; Jin, W.; Chen, X. Facile synthesis of hierarchically aloe-like gold micro/nanostructures for ultrasensitive DNA recognition. *Biosens. Bioelectron.* **2013**, *49*, 184–191. [[CrossRef](#)] [[PubMed](#)]
82. Qin, X.; Miao, Z.; Fang, Y.; Zhang, D.; Ma, J.; Zhang, L.; Chen, Q.; Shao, X. Preparation of dendritic nanostructures of silver and their characterization for electroreduction. *Langmuir* **2012**, *28*, 5218–5226. [[CrossRef](#)] [[PubMed](#)]
83. Sakai, N.; Fujiwara, Y.; Arai, M.; Yu, K.; Tatsuma, T. Electrodeposition of gold nanoparticles on ITO: Control of morphology and plasmon resonance-based absorption and scattering. *J. Electroanal. Chem.* **2009**, *628*, 7–15. [[CrossRef](#)]
84. Sanzò, G.; Taurino, I.; Puppo, F.; Antiochia, R.; Gorton, L.; Favero, G.; Mazzei, F.; Carrara, S.; De Micheli, G. A bimetallic nanocoral Au decorated with Pt nanoflowers (bio)sensor for H<sub>2</sub>O<sub>2</sub> detection at low potential. *Methods* **2017**, *129*, 89–95. [[CrossRef](#)] [[PubMed](#)]
85. Sanzò, G.; Taurino, I.; Antiochia, R.; Gorton, L.; Favero, G.; Mazzei, F.; De Micheli, F.; Carrara, S. Bubble electrodeposition of gold porous nanocorals for the enzymatic and non-enzymatic detection of glucose. *Bioelectrochemistry* **2016**, *112*, 125–131. [[CrossRef](#)] [[PubMed](#)]
86. Argoubi, W.; Saadaoui, M.; Ben Aoun, S.; Raouafi, N. Optimized design of a nanostructured SPCE-based multipurpose biosensing platform formed by ferrocene-tethered electrochemically-deposited cauliflower-shaped gold nanoparticles. *Beilstein J. Nanotechnol.* **2015**, *6*, 1840–1852. [[CrossRef](#)] [[PubMed](#)]
87. Li, M.; Zhao, G.; Geng, R.; Hu, H. Facile electrocatalytic redox of hemoglobin by flower-like gold nanoparticles on boron-doped diamond surface. *Bioelectrochemistry* **2008**, *74*, 217–221. [[CrossRef](#)] [[PubMed](#)]
88. Taurino, I.; Sanzò, G.; Mazzei, F.; Favero, G.; De Micheli, G.; Carrara, S. Fast synthesis of platinum nanopetals and nanospheres for highly-sensitive non-enzymatic detection of glucose and selective sensing of ions. *Sci. Rep.* **2015**, *5*, 15277. [[CrossRef](#)] [[PubMed](#)]
89. Taurino, I.; Massa, S.; Sanzò, G.; Aleman, J.; Flavia, B.; Shin, S.R.; Zhang, Y.S.; Dokmeci, M.R.; De Micheli, G.; Carrara, S.; et al. Platinum nanopetal-based potassium sensors for acute cell death monitoring. *RSC Adv.* **2016**, *6*, 40517–40526. [[CrossRef](#)]
90. Bu, Y.; Lee, S.-W. Flower-like gold nanostructures electrodeposited on indium tin oxide (ITO) glass as a SERS-active substrate for sensing dopamine. *Microchim. Acta* **2015**, *182*, 1313–1321. [[CrossRef](#)]
91. Zhang, H.; Xu, J.-J.; Chen, H.-Y. Shape-controlled gold nanoarchitectures: Synthesis, superhydrophobicity, and electrocatalytic properties. *J. Phys. Chem. C* **2008**, *112*, 13886–13892. [[CrossRef](#)]
92. Delshadi-Jahromi, N.; Nazari-Vanani, R.; Yadegaric, H.; Sattarahmady, N.; Hatame, G.R.; Heli, H. Label-free ultrasensitive electrochemical genosensing of *Trichomonas vaginalis* using anisotropic-shaped gold nanoparticles as a platform, a repeated sequence of the parasite DNA as a probe, and toluidine blue as a redox marker. *Sens. Actuators B* **2018**, *273*, 234–241. [[CrossRef](#)]
93. Nazari-Vanania, R.; Sattarahmady, N.; Yadegari, H.; Delshadi, N.; Hatam, G.R.; Helia, H. Electrochemical quantitation of *Leishmania infantum* based on detection of its kDNA genome and transduction of non-spherical gold nanoparticles. *Anal. Chim. Acta* **2018**, *1041*, 40–49. [[CrossRef](#)] [[PubMed](#)]

94. Moradi, M.; Sattarahmady, N.; Rahi, A.; Hatam, G.R.; RezayatSorkhabadi, S.M.; Heli, H. A label-free, PCR-free and signal-on electrochemical DNA biosensor for *Leishmania major* based on gold nanoleaves. *Talanta* **2016**, *161*, 48–53. [[CrossRef](#)] [[PubMed](#)]
95. Sattarahmady, N.; Rahi, A.; Heli, H. A signal-on built in-marker electrochemical aptasensor for human prostate-specific antigen based on a hairbrush-like gold nanostructure. *Sci. Rep.* **2017**, *7*, 11238. [[CrossRef](#)] [[PubMed](#)]
96. Liu, Y.; Xu, L.-P.; Wang, S.; Yang, W.; Wen, Y.; Zhang, X. An ultrasensitive electrochemical immunosensor for apolipoprotein E4 based on fractal nanostructures and enzyme amplification. *Biosens. Bioelectron.* **2015**, *71*, 396–400. [[CrossRef](#)] [[PubMed](#)]
97. Zhang, P.; Chen, L.; Xu, T.; Liu, H.; Liu, X.; Meng, J.; Yang, G.; Jiang, L.; Wang, S. Programmable fractal nanostructured interfaces for specific recognition and electrochemical release of cancer cells. *Adv. Mater.* **2013**, *25*, 3566–3570. [[CrossRef](#)] [[PubMed](#)]
98. Elbourne, A.; Coyle, V.E.; Truong, V.K.; Sabri, Y.M.; Kandjani, A.E.; Bhargava, S.K.; Ivanova, E.P.; Crawford, R.J. Multi-directional electrodeposited gold nanopikes for antibacterial surface application. *Nanoscale Adv.* **2019**, *1*, 203–212. [[CrossRef](#)]
99. Mahshid, S.; Mephram, A.H.; Mahshid, S.S.; Burgess, I.B.; Safaei, T.S.; Sargent, E.H.; Kelley, S.O. Mechanistic Control of the Growth of Three-Dimensional Gold Sensors. *J. Phys. Chem. C* **2016**, *120*, 21123–21132. [[CrossRef](#)]
100. Soleymani, L.; Fang, Z.; Sargent, E.H.; Kelley, S.O. Programming the detection limits of biosensors through controlled nanostructuring. *Nat. Nanotechnol.* **2009**, *4*, 844–848. [[CrossRef](#)] [[PubMed](#)]
101. Soleymani, L.; Fang, Z.; Kelley, S.O.; Sargent, E.H. Integrated nanostructures for direct detection of DNA at attomolar concentrations. *Appl. Phys. Lett.* **2009**, *95*, 143701. [[CrossRef](#)]
102. Soleymani, L.; Fang, Z.; Sun, X.; Yang, H.; Taft, B.J.; Sargent, E.H.; Kelley, S.O. Nanostructuring of patterned microelectrodes To enhance the sensitivity of electrochemical nucleic acids detection. *Angew. Chem. Int. Ed.* **2009**, *48*, 8457–8460. [[CrossRef](#)] [[PubMed](#)]
103. Fang, Z.; Soleymani, L.; Pampalakis, G.; Yoshimoto, M.; Squire, J.A.; Sargent, E.H.; Kelley, S.O. Direct profiling of cancer biomarkers in tumor tissue using a multiplexed nanostructured microelectrode integrated circuit. *ACS Nano* **2009**, *3*, 3207–3213. [[CrossRef](#)] [[PubMed](#)]
104. Bin, X.; Sargent, E.H.; Kelley, S.O. Nanostructuring of sensors determines the efficiency of biomolecular capture. *Anal. Chem.* **2010**, *82*, 5928–5931. [[CrossRef](#)] [[PubMed](#)]
105. Vasilyeva, E.; Lam, B.; Fang, Z.; Minden, M.D.; Sargent, E.H.; Kelley, S.O. Direct Genetic analysis of ten cancer cells: Tuning sensor structure and molecular probe design for efficient mRNA capture. *Angew. Chem. Int. Ed.* **2011**, *50*, 4137–4141. [[CrossRef](#)] [[PubMed](#)]
106. Das, J.; Kelley, S.O. Protein detection using arrayed microsensor chips: Tuning sensor footprint to achieve ultrasensitive readout of CA-125 in serum and whole blood. *Anal. Chem.* **2011**, *83*, 1167–1172. [[CrossRef](#)] [[PubMed](#)]
107. Lam, B.; Fang, Z.; Sargent, E.H.; Kelley, S.O. Polymerase chain reaction-free, sample-to-answer bacterial detection in 30 min with integrated cell lysis. *Anal. Chem.* **2012**, *84*, 21–25. [[CrossRef](#)] [[PubMed](#)]
108. Soleymani, L.; Fang, Z.; Lam, B.; Bin, X.; Vasilyeva, E.; Ross, A.J.; Sargent, E.H.; Kelley, S.O. Hierarchical nanotextured microelectrodes overcome the molecular transport barrier To achieve rapid, direct bacterial detection. *ACS Nano* **2011**, *5*, 3360–3366. [[CrossRef](#)] [[PubMed](#)]
109. Narwala, V.; Kumar, P.; Joon, P.; Pundira, C.S. Fabrication of an amperometric sarcosine biosensor based on sarcosine oxidase/chitosan/CuNPs/c-MWCNT/Au electrode for detection of prostate cancer. *Enzyme Microb. Technol.* **2018**, *113*, 44–51. [[CrossRef](#)] [[PubMed](#)]
110. Wang, Y.; Zhang, L.; Shen, L.; Ge, S.; Yu, J.; Yan, M. Electrochemiluminescence DNA biosensor based on the use of gold nanoparticle modified graphite-like carbon nitride. *Microchim. Acta* **2017**, *184*, 2587–2596. [[CrossRef](#)]
111. Wu, F.; Huang, T.; Hu, Y.; Yang, X.; Xie, Q. One-pot electrodeposition of a composite film of glucose oxidase, imidazolium alkoxysilane and chitosan on a reduced graphene oxide–Pt nanoparticle/Au electrode for biosensing. *J. Electroanal. Chem.* **2016**, *781*, 296–303. [[CrossRef](#)]
112. Yagati, A.K.; Lee, G.-Y.; Ha, S.; Chang, K.-A.; Pyun, J.-C.; Cho, S. Impedimetric tumor necrosis factor- $\alpha$  sensor based on a reduced graphene oxide nanoparticle-modified electrode array. *J. Nanosci. Nanotechnol.* **2016**, *16*, 11921–11927. [[CrossRef](#)]

113. Yu, G.; Wu, W.; Pan, X.; Zhao, Q.; Wei, X.; Lu, Q. High sensitive and selective sensing of hydrogen peroxide released from *Pheochromocytoma* cells based on Pt-Au bimetallic nanoparticles electrodeposited on reduced graphene sheets. *Sensors* **2015**, *15*, 2709–2722. [[CrossRef](#)] [[PubMed](#)]
114. Yang, C.-Y.; Tsai, T.-H.; Chen, S.-M.; Lou, B.-S.; Liu, X. Development of a multiple biosensor and its application of biofuel cell. *Int. J. Electrochem. Sci.* **2015**, *10*, 579–588.
115. Wu, X.; Zhong, X.; Chai, Y.; Yuan, R. Electrochemiluminescence acetylcholine biosensor based on biofunctional AMs-AChE-ChO biocomposite and electrodeposited graphene-Au-chitosan nanocomposite. *Electrochim. Acta* **2014**, *147*, 735–742. [[CrossRef](#)]
116. Zheng, Y.; Wang, A.; Lina, H.; Fub, L.; Cai, W. A sensitive electrochemical sensor for direct Phoxim detection based on electrodeposited reduced graphene oxide-gold nanocomposite. *RSC Adv.* **2015**, *5*, 15425–15430. [[CrossRef](#)]
117. Shi, L.; Yu, Y.; Chen, Z.; Zhang, L.; He, S.; Shia, Q.; Yang, H. A label-free hemin/G-quadruplex DNAzyme biosensor developed on electrochemically modified electrodes for detection of a HBV DNA segment. *RSC Adv.* **2015**, *5*, 11541–11548. [[CrossRef](#)]
118. Numnuam, A.; Thavarungkul, P.; Kanatharana, P. An amperometric uric acid biosensor based on chitosan-carbon nanotubes electrospun nanofiber on silver nanoparticles. *Anal. Bioanal. Chem.* **2014**, *406*, 3763–3772. [[CrossRef](#)] [[PubMed](#)]
119. Zhao, Y.; Fan, L.; Ren, J.; Hong, B. Gold nanoclusters electrodeposited on multi-walled carbon nanotubes: Enhanced electrocatalytic activity of hemoglobin. *J. Solid State Electrochem.* **2014**, *18*, 1099–1109. [[CrossRef](#)]
120. Li, G.; Li, T.; Deng, Y.; Cheng, Y.; Shi, F.; Sun, W.; Sun, Z. Electrodeposited nanogold decorated graphene modified carbon ionic liquid electrode for the electrochemical myoglobin biosensor. *J. Solid State Electrochem.* **2013**, *17*, 2333–2340. [[CrossRef](#)]
121. Benvidi, A.; Dehghani-Firouzabadi, A.; Mazloun-Ardakani, M.; Fatemeh Mirjalili, B.-B.; Zare, R. Electrochemical deposition of gold nanoparticles on reduced graphene oxide modified glassy carbon electrode for simultaneous determination of levodopa, uric acid and folic acid. *J. Electroanal. Chem.* **2015**, *736*, 22–29. [[CrossRef](#)]
122. Yiwei, X.; Wen, Z.; Jiyong, S.; Xiaobo, Z.; Yanxiao, L.; Tahir, H.E.; Xiaowei, H.; Zhihua, L.; Xiaodong, Z.; Xuetao, H. Electrodeposition of gold nanoparticles and reduced graphene oxide on an electrode for fast and sensitive determination of methylmercury in Fish. *Food Chem.* **2017**, *237*, 423–430.
123. Chu, Z.; Liu, Y.; Xu, Y.; Shi, L.; Peng, J.; Jin, W. In-situ fabrication of well-distributed gold nanocubes on thiol graphene as a third-generation biosensor for ultrasensitive glucose detection. *Electrochim. Acta* **2015**, *176*, 162–171. [[CrossRef](#)]
124. Zhao, W.; Yang, H.; Xu, S.; Cai, J.; Luo, J.; Wei, W.; Liu, X.; Zhu, Y. Preparation of molecularly imprinted polymer/Au nanohybrids as an effective biosensing material. *Colloids Surf. A* **2018**, *555*, 95–102. [[CrossRef](#)]
125. Karazehir, T.; Guler Gokce, Z.; Ates, M.; Sarac, A.S. Gold nanoparticle/nickel oxide/poly(pyrrole-*N*-propionic acid) hybrid multilayer film: Electrochemical study and its application in biosensing. *eXPRESS Polym. Lett.* **2017**, *11*, 449–466. [[CrossRef](#)]
126. Hui, Y.; Ma, X.; Qu, F.; Chen, F.; Yu, J.; Gao, Y. Electropolymerization of carboxymethyl- $\beta$ -cyclodextrin based on co-electrodeposition gold nanoparticles electrode: Electrocatalysis and nonenzymatic glucose sensing. *J. Solid State Electrochem.* **2016**, *20*, 1377–1389. [[CrossRef](#)]
127. Miao, Z.; Wang, P.; Zhong, M.; Yang, M.; Xua, Q.; Hao, S.; Hu, X. Development of a glucose biosensor based on electrodeposited gold nanoparticles-polyvinylpyrrolidone-polyaniline nanocomposites. *J. Electroanal. Chem.* **2015**, *756*, 153–160. [[CrossRef](#)]
128. Che, X.; Yuan, R.; Chai, Y.; Ma, L.; Li, W.; Li, J. Hydrogen peroxide sensor based on horseradish peroxidase immobilized on an electrode modified with DNA-L-cysteine-gold-platinum nanoparticles in polypyrrole film. *Microchim. Acta* **2009**, *167*, 159–165. [[CrossRef](#)]
129. Zhao, H.; He, H.; Shi, L.; Cai, X.; Lia, H.; Lan, M.; Zhang, Q. Electrochemical detection of 4-(methylnitrosamino)-1-(3-pyridyl)-1-butanone using a cytochrome P450 2E1 decorated biosensor. *J. Electroanal. Chem.* **2018**, *816*, 62–67. [[CrossRef](#)]
130. Mohtar, L.G.; Aranda, P.; Messina, G.A.; Nazareno, M.A.; Pereira, S.V.; Raba, J.; Bertolino, F.A. Amperometric biosensor based on laccase immobilized onto a nanostructured screen-printed electrode for determination of polyphenols in propolis. *Microchem. J.* **2019**, *144*, 13–18. [[CrossRef](#)]
131. Karyakin, A.A. Prussian blue and its analogues: Electrochemistry and analytical applications. *Electroanalysis* **2001**, *13*, 813–819. [[CrossRef](#)]



132. Chao, L.; Wang, W.; Dai, M.; Ma, Y.; Sun, L.; Qin, X.; Xie, Q. Step-by-step electrodeposition of a high-performance Prussian blue-gold nanocomposite for H<sub>2</sub>O<sub>2</sub> sensing and glucose biosensing. *J. Electroanal. Chem.* **2016**, *778*, 66–73. [[CrossRef](#)]
133. Tian, R.; Chen, X.; Liu, D.; Yao, C. A Sensitive Biosensor for Determination of Cu<sup>2+</sup> by One-step Electrodeposition. *Electroanalysis* **2016**, *28*, 1617–1624. [[CrossRef](#)]
134. Wang, B.; Jin, X.; Zhao, H.; Wang, N.; Li, X.; Ni, R.; Liu, Y. An amperometric β-glucan biosensor based on the immobilization of bi-enzyme on Prussian blue–chitosan and gold nanoparticles–chitosan nanocomposite films. *Biosens. Bioelectron.* **2014**, *55*, 113–119. [[CrossRef](#)] [[PubMed](#)]
135. Mauritz, K.A.; Moore, R.B. State of understanding of Nafion. *Chem. Rev.* **2004**, *104*, 4535–4585. [[CrossRef](#)] [[PubMed](#)]
136. Thangavel, S.; Ramaraj, R. Polymer membrane stabilized gold nanostructures modified electrode and its application in nitric oxide detection. *J. Phys. Chem. C* **2008**, *112*, 19825–19830. [[CrossRef](#)]
137. Krajewska, B. Application of chitin- and chitosan-based materials for enzyme immobilizations: A review. *Enzyme Microb. Technol.* **2004**, *35*, 126–139. [[CrossRef](#)]
138. Dagar, K.; Pundir, C. Covalent immobilization of lactate oxidase onto zirconia coated silica nanoparticles/chitosan hybrid film for amperometric determination of lactate. *Biochem. Anal. Biochem.* **2016**, *5*, 301–309.
139. Zeng, X.; Li, X.; Xing, L.; Liu, X.; Luo, S.; Wei, W.; Kong, B.; Li, Y. Electrodeposition of chitosan–ionic liquid–glucose oxidase biocomposite onto nano-gold electrode for amperometric glucose sensing. *Biosens. Bioelectron.* **2009**, *24*, 2898–2903. [[CrossRef](#)] [[PubMed](#)]
140. Feng, D.; Wang, F.; Chen, Z. Electrochemical glucose sensor based on one-step construction of gold nanoparticle–chitosan composite film. *Sens. Actuators B* **2009**, *138*, 539–544. [[CrossRef](#)]
141. Wang, Y.; Wu, Y.; Wang, J.; Di, J. Disposable superoxide anion biosensor based on superoxide dismutase entrapped in silica sol–gel matrix at gold nanoparticles modified ITO electrode. *Bioprocess Biosyst. Eng.* **2009**, *32*, 531–536. [[CrossRef](#)] [[PubMed](#)]
142. Wang, L.; Mao, W.; Ni, D.; Di, J.; Wu, Y.; Tu, Y. Direct electrodeposition of gold nanoparticles onto indium/tin oxide film coated glass and its application for electrochemical biosensor. *Electrochem. Commun.* **2008**, *10*, 673–676. [[CrossRef](#)]
143. Du, J.; Yu, X.; Di, J. Comparison of the direct electrochemistry of glucose oxidase immobilized on the surface of Au, CdS, and ZnS nanostructures. *Biosens. Bioelectron.* **2012**, *37*, 88–93. [[CrossRef](#)] [[PubMed](#)]
144. Breslauer, K.J.; Frank, R.; Blöcker, H.; Marky, L.A. Predicting DNA duplex stability from the base sequence. *Proc. Natl. Acad. Sci. USA* **1986**, *83*, 3746–3750. [[CrossRef](#)] [[PubMed](#)]



© 2019 by the author. Licensee MDPI, Basel, Switzerland. This article is an open access article distributed under the terms and conditions of the Creative Commons Attribution (CC BY) license (<http://creativecommons.org/licenses/by/4.0/>).